February 2022

CHARACTERIZATION OF PRODUCED WATER IN THE PERMIAN BASIN FOR POTENTIAL BENEFICIAL USE

NM WRRI Technical Completion Report No. 398

Pei Xu
Yanyan Zhang
Wenbin Jiang
Lei Hu
Xuesong Xu
Kenneth C. Carroll
Naima Khan

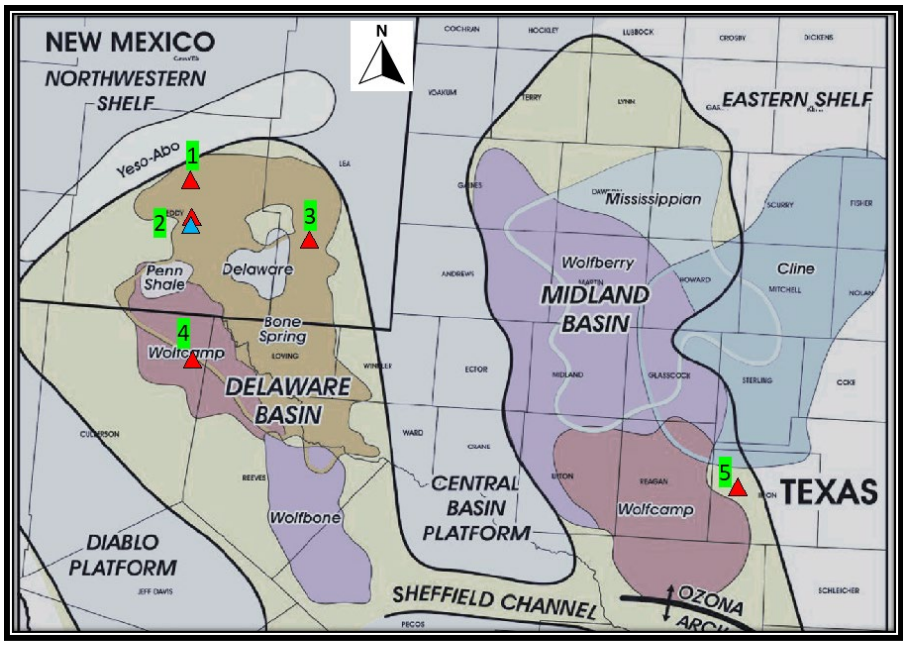

▲ Produced water sampling point

▲ Pecos River water sampling point

New Mexico Water Resources Research Institute
New Mexico State University
MSC 3167, P.O. Box 30001
Las Cruces, New Mexico 88003-0001
(575) 646-4337 email: nmwrri@nmsu.edu

CHARACTERIZATION OF PRODUCED WATER IN THE PERMIAN BASIN FOR POTENTIAL BENEFICIAL USE

By

Pei Xu, Yanyan Zhang, Wenbin Jiang, Lei Hu, Xuesong Xu
Department of Civil Engineering, New Mexico State University

Kenneth C. Carroll, Naima Khan
Department of Plant and Environmental Science, New Mexico State University

TECHNICAL COMPLETION REPORT
Account Number 13352
Technical Completion Report #398

February 2022

New Mexico Water Resources Research Institute
In cooperation with
Department of Civil Engineering
and
Department of Plant and Environmental Science
New Mexico State University

The research on which this report is based was financed in part by The New Mexico Universities Produced Water Synthesis Project and by the U.S. Department of the Interior, Geological Survey, through the New Mexico Water Resources Research Institute.

Page Intentionally Left Blank

DISCLAIMER

The purpose of the NM Water Resources Research Institute (NM WRRI) technical reports is to provide a timely outlet for research results obtained on projects supported in whole or in part by the institute. Through these reports the NM WRRI promotes the free exchange of information and ideas and hopes to stimulate thoughtful discussions and actions that may lead to resolution of water problems. The NM WRRI, through peer review of draft reports, attempts to substantiate the accuracy of information contained within its reports, but the views expressed are those of the authors and do not necessarily reflect those of the NM WRRI or its reviewers. Contents of this publication do not necessarily reflect the views and policies of the Department of the Interior, nor does the mention of trade names or commercial products constitute their endorsement by the United States government.

ABSTRACT

The rapid development of the unconventional oil and gas industry has promoted economic growth in the southwestern region of the United States. One of the major barriers for using treated produced water as an alternative water source is the lack of a comprehensive assessment of produced water quality and environmental toxicity. In this study, we employed advanced analytical methods to measure more than 300 targeted analytes including inorganics (e.g., salts, major ions, and metals), organics (e.g., total organic carbon, volatile and semi-volatile organic contaminants), and radionuclides in produced water. *In vitro* assays were developed as valuable tools for the toxicity assessment of produced water. Overall, an understanding of the physicochemical and toxicological properties of produced water is critical for establishing management practices, proper risk assessment, spill response, treatment, and beneficial use applications.

Keywords: Water quality; produced water characterization; Permian Basin; Pecos River; water reuse

ACKNOWLEDGMENTS

This study was financially supported by New Mexico Water Resources Research Institute and the New Mexico Produced Water Research Consortium. We are very grateful for the technical support provided by Mr. Ryan Hall and Matthias Sayer with NGL Partners LP; the contribution of Mr. Mike Hightower, the Program Director of New Mexico Produced Water Research Consortium; and Consortium members for sharing data, technical review, and their invaluable expertise.

PUBLICATIONS RELATED TO PROJECT

Jiang, W., Xu, X., Hall, R., Zhang, Y., Carroll, K.C., Ramos, F., Engle, M.A., Lin, L., Wang, H., Sayer, M., and Xu, P. 2022. Characterization of produced water and surrounding surface water in the Permian Basin, the United States. Journal of Hazardous Materials, 430, 128409. Available at: https://doi.org/10.1016/j.jhazmat.2022.128409

Hu, L., Jiang, W., Xu, X., Wang, H., Carroll, K.C., Xu, P., and Zhang, Y. 2022. Toxicological characterization of produced water from the Permian Basin. Science of the Total Environment, 815, 152943. Available at: http://dx.doi.org/10.1016/j.scitotenv.2022.152943

TABLE OF CONTENTS

LIST OF TABLES

LIST OF FIGURES

LIST OF ACRONYMS

BTEX	benzene, toluene, ethylbenzene, and xylene
CID	collision induced dissociation
COD	chemical oxygen demand
DBE	double bond equivalence
DOC	dissolved organic carbon
DOM	dissolved organic matter
DRO	diesel range organics
EC_{50} values	the concentration that results in 50% of growth rate inhibition
EOR	enhanced oil recovery
EPA	Environmental Protection Agency
Ex/Em	excitation/emission
FEEM	fluorescence excitation-emission matrix
FT ICR-MS	Fourier-transform ion cyclotron resonance mass spectrometry
GC	gas chromatography
gDNA	genomic DNA
GRO	gasoline range organics
HF	hydraulic fracturing
HPLC	high-performance liquid chromatography
IC	ion chromatography
ICP-MS	inductively coupled plasma mass spectroscopy
ICP-OES	inductively coupled plasma optical emission spectroscopy
LC-MS/MS	liquid chromatography-tandem mass spectrometry
MBAS	methylene blue active substances
MRO	motor oil range organics
MS	mass spectrometry
ND	not detected
NIST	National Institute of Standards and Technology
NORM	naturally-occurring radioactive material
NPDES	National Pollutant Discharge Elimination System

O&G	oil and gas
OTUs	operational taxonomic units
PAHs	polycyclic aromatic hydrocarbons
PTFE	polytetrafluoroethylene
PW	produced water
QIIME2	Quantitative Insights into Microbial Ecology
RO	reverse osmosis
SVOCs	semi-volatile organic compounds
SWD	saltwater disposal
TDS	total dissolved solids
TICs	tentatively identified compounds
TOC	total organic carbon
TPH	total petroleum hydrocarbons
TSS	total suspended solids
USGS	United States Geological Survey
VOCs	volatile organic compounds
WET	whole effluent toxicity

1. INTRODUCTION

The rapid development of the unconventional oil and gas (O&G) industry has promoted economic growth and generated large volumes of produced water (PW) in the southwestern region of the United States (U.S. EIA, 2021). Primarily, PW is naturally occurring water that emerges from the ground during the production of oil or gas (also known as formation water). Additionally, PW may include water injected into the formation during well treatment or enhanced oil recovery (EOR), as well as flowback water that returns to the surface after hydraulic fracturing (HF) (GWPC, 2019; Scanlon et al., 2017). An estimated $3{,}180 \times 10^6$ m^3 (20 billion barrels) of PW will be generated by onshore O&G activities in the United States in 2022 (IHS Markit, 2020). Such large volumes of PW require appropriate management to reduce disposal costs and environmental impacts. Currently, major PW management methods include saltwater disposal (SWD) well injection, reinjection for EOR, and reuse for HF; only a very small percentage of PW (1.3% in 2017) is used outside the O&G field for irrigation and dust control on roads (Jiang et al., 2021b; U.S. EPA, 2020; Veil, 2020).

Following appropriate treatment, treated PW could prove to be an alternative water supply for other industrial applications as well as serving to reduce stress on local water supplies. PW recycling for HF has been implemented as an economically attractive and environmentally friendly method by the O&G industry (Scanlon et al., 2020a). One challenge for PW recycling is temporally and geographically matching water demand for HF with PW supply (Jiang et al., 2021b), and that PW volume may exceed HF water demand in some areas, such as in the Permian Basin (Scanlon et al., 2020a). PW could also be treated and beneficially reused outside the O&G field to alleviate local water stress. For example, the Permian Basin is in a semi-arid region where treated PW can be used as an alternative water source to replace and augment freshwater supplies. Scanlon et al. estimated that PW, after meeting the HF water demand, if it were treated and used, could represent <1%, 5%, and 11% of irrigation water demand in Eddy, Lea, and Pecos counties, respectively, the highest irrigation counties in the Permian Delaware Basin (Scanlon et al., 2020b).

Use of treated PW for agriculture or wildlife is currently allowed west of the 98th meridian under the Oil and Gas Extraction Effluent Guidelines and Standards (40 CFR Part 435 Subpart E) in the United States. PW reuse outside the O&G field for agriculture and wildlife propagation

primarily occurs in California and Wyoming because some PW in these regions has lower total dissolved solids (TDS) and may only need moderate treatment (Navarro et al., 2016; U.S. EPA, 2020). Constituents in PW vary with geographic location, reservoir lithology, geologic history, the type of hydrocarbon product being produced, and well age, which makes it difficult to fully characterize PW composition, including adequately understanding spatial and temporal variability in the production (volumes) and composition (Oetjen et al., 2018; Wang et al., 2019). Typically, PW is highly saline and could contain many different constituents such as suspended particles, dissolved mineral salts, organic compounds (e.g., volatile and semi-volatile organic compounds (VOCs and SVOCs), petroleum hydrocarbons, organic acids, and oils), naturally-occurring radioactive material (NORM), other inorganic constituents (e.g., sulfide and ammonia), chemical additives and their transformational byproducts during well treatment or from the interactions with formation water (Jiang et al., 2021a; Rodriguez et al., 2020). Extensive treatment is required to remove these constituents for safe reuse of treated PW, which can include settling, media filtration, coagulation, chemical precipitation, adsorption, biological treatment, membrane desalination, thermal distillation, and advanced oxidation processes (Chen et al., 2021; Chen et al., 2022; Geza et al., 2018; Hickenbottom et al., 2013; Hu et al., 2020; Lin et al., 2020; Ma et al., 2018; Xu and Drewes, 2006; Xu et al., 2008a; Xu et al., 2008b).

One of the barriers to using treated PW as an alternative water source is the lack of comprehensive characterization of PW quality (Scanlon et al., 2020b). To date, most studies devoted to PW characterization are focused on the Appalachian Basin (Danforth et al., 2020). Some previous research on the Niobrara (Oetjen et al., 2018), the Barnett (Wang et al., 2019), the Bakken (Shrestha et al., 2018), and the Eagle Ford (Hildenbrand et al., 2018) formations also exist. The Permian Basin in southeastern New Mexico and western Texas (Fig. 1a) is the most productive oil province in the U.S., and accounted for almost 60% of onshore oil production in July 2021 (U.S. EIA, 2021). However, there are limited studies focused on the characterization of PW in the Permian Basin, especially the PW from unconventional wells. Most PW samples from the Permian Basin in the United States Geological Survey (USGS) database (approximately 3,800 datasets for the Permian out of 114,993 total datasets in the 'USGSPWDBv2.3n.csv' file) were collected before 2002, and primarily from conventional wells. Only 39 samples (out of 3,800 datasets) are from 2016, with limited inorganic information (Chaudhary et al., 2019; Engle et al., 2016; USGS, 2021). Our previous research identified VOCs in eight unconventional PW

samples; however, it was limited in scope to the Midland Basin (the eastern portion of the Permian Basin, Texas) and did not fully characterize PW samples to a level sufficient to support hazard and risk assessment. The same limited scope of analysis and sampling is reflected in the broader literature (Hu et al., 2020; Rodriguez et al., 2020; Thacker et al., 2015). Thus, comprehensive chemical characterization and risk assessment of PW is necessary for potential treatment and beneficial use outside the O&G field in the Permian Basin.

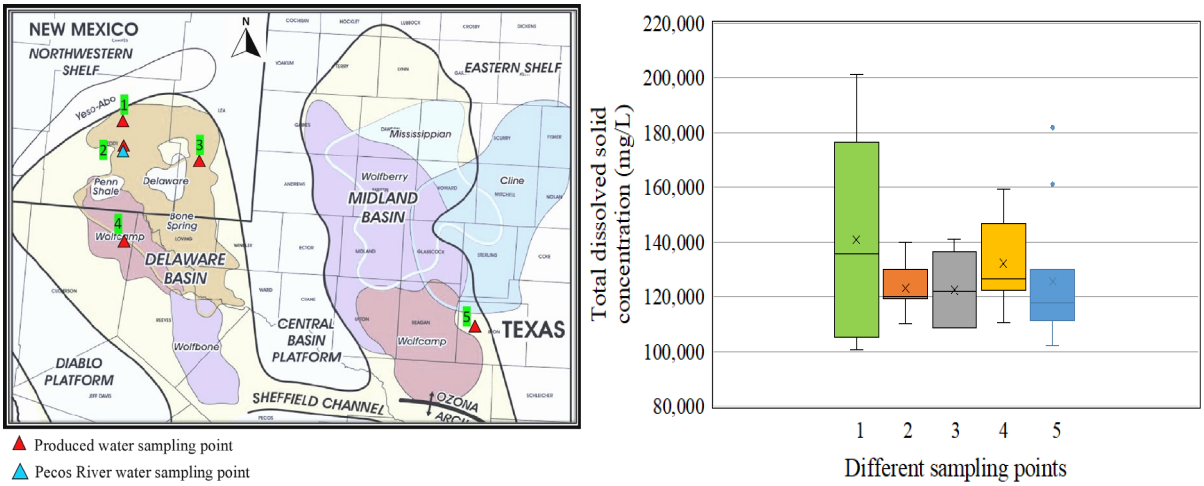

Fig. 1. (a) Sampling points of PW and Pecos River water in this study. (b) TDS distribution of PW at different sampling points. "x" represents Mean value, "–" from top to bottom represent Max, Median, and Min values, respectively. Two dots in Sampling Point 5 are outliers during the statistical analysis using the box and whisker plot. For PW samples: Point 1 (7 samples) TDS: 140,891 ± 38,516 mg/L; Point 2 (12 samples) TDS: 123,298 ± 8,752 mg/L; Point 3 (5 samples) TDS: 122,440 ± 14,217 mg/L; Point 4 (12 samples) TDS: 132,044 ± 15,933 mg/L; Point 5 (10 samples) TDS: 125,439 ± 25,368 mg/L. Permian Basin County map is cited from (Shaleexperts, 2021).

In this study, we analyzed the physical, chemical, and biological characteristics of PW samples from five locations in the Permian Basin and water samples from one location on the Pecos River (the river flowing through the Permian Basin) near Carlsbad, New Mexico (Fig. 1a). Twenty-four PW samples were collected from the Permian Basin in New Mexico and Texas, 14 samples (PW-NM) from Sampling Point 2, and 10 samples (PW-TX) from Sampling Point 5 as shown in Fig. 1a. Samples were analyzed for wet chemistry, inorganics, organics, and radionuclides. Among these 24 samples, ten samples (PW-NM) were collected from January 2020 to September 2020 to monitor the temporal change of PW quality (Point 2 in Fig. 1a). Along with these ten PW samples (PW-NM), ten Pecos River samples (NM) were collected within the same period to characterize the background surface water quality (Point 2 in Fig. 1a).

These temporal samples (ten PW-NM samples from Point 2 in Fig. 1a) were quantitatively analyzed for more than 300 targeted analytes, including wet chemistry, inorganics, radionuclides, organics such as VOCs, SVOCs, total petroleum hydrocarbons and organic acids, oil and grease, pesticides/herbicides, dioxins, and tentatively identified compounds. We also obtained data (wet chemistry and inorganics) from an additional 22 PW samples from SWD wells (Points 1, 3, and 4 in Fig. 1a) and then combined all the data (in total 46 samples) for statistical analyses.

In addition to target analysis, two PW samples, one river water sample, one groundwater sample, and one tap water sample were collected from the sampling location Point 2 in Carlsbad, NM, for non-target analysis of organic constituents using high-resolution mass spectroscopy. Three PW samples from SWD wells and one river water collected in Point 2 were analyzed for microbial community profile and acute and chronic toxicity.

This study is a first step toward a better understanding of PW quality in the Permian Basin. The objective of this study and our future research is to support the O&G industry, regulators, and stakeholders with information for risk-based assessment and design of optimal methods for treatment and potential beneficial use of treated PW outside the O&G industry.

2. MATERIALS AND METHODS

2.1. Water sample collection

This study included 46 PW samples from the Permian Basin. Fig. 1a identifies sampling locations. Fig. 1b describes the TDS distribution for samples from each sampling point with mean, max, min, and standard deviation of TDS concentrations. Twenty-four PW samples (14 from the Delaware Basin in NM; and 10 from the Midland Basin in TX) were collected from unconventional reservoirs and analyzed by the authors. The information (wet chemistry and inorganics) for the other 22 PW samples was provided by industry collaborators in the Permian Basin. Samples were all from unconventional wells and collected from the wellhead, separator, PW storage tank/pond, and the back end of the SWD tank battery system. To track the temporal change of general water quality, ten PW-NM-SWD samples from the back end of a SWD tank battery system and ten Pecos RW-NM samples (Point 2 in Fig. 1a) were collected between

January to September 2020 from the Delaware Basin (western subbasin of the Permian Basin), near Carlsbad, New Mexico.

Samples for wet chemistry, inorganic, and radionuclide analyses were collected in sterile plastic bottles. Samples for organic analyses were collected in method-specific bottles provided by the analytical laboratories. All samples were stored at 4°C and transported to the labs on the same day under chain of custody. All sample collection, preservation, shipping, and analyses followed the United States Environmental Protection Agency (EPA) guidance and standard practices.

2.2 Wet chemistry, inorganic, and radionuclides analyses

Total dissolved solids (TDS) and total suspended solids (TSS) were measured by EPA standard methods 2540C and 2540D (gravimetric method) using 0.15 μm filters. Total organic carbon (TOC) and dissolved organic carbon (DOC, using 0.45 μm filters) were measured using a TOC-V CSH Total Organic Carbon Analyzer (Shimadzu, Japan), following EPA method 415.3. The TOC procedure allows for removal of settleable solids and any free oil layer to prevent the clogging of valves, tubing, and injection needles. The suspended particles are included in the TOC measurement. pH was measured using a benchtop multi-parameter meter (pH/con 300 Meter, Oakton Instruments, IL, USA). Ammonia was measured using a Hach DR6000 spectrophotometer with the salicylate method 10031 (Hach, CO, USA). Chemical oxygen demand (COD) was measured using Hach COD test kits (Hach, CO, USA). Alkalinity was measured using Hach alkalinity test kits (Hach, CO, USA). Major anions were measured using ion chromatography (IC; Dionex ICS-2100, Thermo Fisher Scientific, CA, USA), using EPA method 300.0. Unfiltered, acidified water samples were used to measure the total metals and trace elements using an inductively coupled plasma optical emission spectroscopy (ICP-OES; Optima 4300 DV, PerkinElmer, MA, USA) and an inductively coupled plasma mass spectroscopy (ICP-MS; Elan DRC-e, PerkinElmer, MA, USA), using EPA methods 200.7 and 200.8, respectively. Methylene blue active substances (surfactants) were analyzed based on EPA method 425.1. Radium-226 and Radium-228 were measured based on EPA methods 903.0 and 904.0, respectively, utilizing gamma spectroscopy. Gross Alpha and Gross Beta counts were based on EPA method 900.0.

2.3 Fluorescence excitation-emission matrix (FEEM) analyses

FEEM was used to analyze the composition of DOC in the water samples. The spectra were obtained by a spectrofluorometer (Aqualog-UV-800-C, Horiba Instruments, NJ, USA). The excitation wavelengths were from 240 to 400 nm with 10 nm steps, and emission wavelengths were from 300 to 550 nm with 2 nm steps. The spectrum of deionized water at the excitation wavelength of 350 nm was recorded as blank, and the equipment was auto zeroed before each analysis. In general, FEEM spectra can be divided into five regions (Jiang et al., 2020): Region I (Ex/Em 240-250/300-330 nm) and Region II (Ex/Em 240-250/330-380 nm): aromatic carbons; Region III (Ex/Em 240-250/380-550 nm): fulvic acid-like compounds; Region IV (Ex/Em 250-400/300-380 nm): microbial byproduct-like materials, such as carbohydrates, aldehydes, and alcohols; and Region V (Ex/Em 250-400/380-550 nm): humic acid-like organics. All spectra were corrected to 1 mg/L DOC with a suitable scale range.

2.4 Targeted organic analyses

Targeted organic analyses were performed by Eurofins Test America. Samples were collected in laboratory-provided method-specific bottles and shipped at 4°C and under chain of custody conditions. VOCs were isolated via purge and trap, and SVOCs (semivolatile organic compounds) were subject to liquid-liquid extraction. They were analyzed using gas chromatography (GC, Agilent 6890) coupled with quadrupole mass spectrometry (MS, Agilent 5973), based on EPA methods 8260C and 8270D, respectively. Total petroleum hydrocarbons (TPH) and organic acids were analyzed using GC coupled with a flame ionization detector (Agilent 5890) based on EPA method 8015D. Pesticides/herbicides were analyzed using GC (Agilent 5890) coupled with an electron capture detector based on EPA method 8081B. Dioxin analysis was performed via high resolution GC/MS in accordance with EPA method 1613B. Blank samples and external/internal standard calibrations were used for quantification. Isotopic dilution was used to aid in quantitation for dioxin analysis.

2.5 Non-targeted organic analyses

Non-targeted organic analyses were performed to identify the unknown compounds in water samples, including two PW samples, a river water sample, a groundwater sample, and a tap

water sample collected from sampling point 2 in Carlsbad, NM (Fig. 1a). Fourier-transform ion cyclotron resonance mass spectrometry (FT ICR-MS) by the National High Magnetic Field Laboratory, University of Florida, was used for the non-target analysis. Water samples were prepared by dissolving the samples in a ratio of 1:1 chloroform to methanol at a concentration of 1 mg/mL. For positive ion mode mass spectral analysis, the stock mixture was further diluted to 0.5 mg/mL in an electrospray ionization solution of 1:2:4 chloroform:methanol:2-propanol containing 0.1% formic acid as an electrospray ionization modifier (for observation of basic compounds). The addition of modifiers to the spray solution facilitates protonation in positive ionization mode. For the analysis of water-soluble organics, the aqueous fraction was diluted 200-fold in positive-ion modes in the electrospray ionization solutions. All solvents were high-performance liquid chromatography (HPLC) grade purchased from Sigma Aldrich (St. Louis, MO). Final prepared solutions were filtered through Acrodisc CR 13 mm syringe filters with 0.2 μm polytetrafluoroethylene (PTFE) membranes (Pall Corporation, Ann Arbor, MI) prior to FT ICR-MS analysis to remove any suspended particulate materials. High-resolution FT ICR-MS was performed with a hybrid linear ion trap FT-ICR mass spectrometer (LTQ FT, Thermo Fisher, San Jose, CA) equipped with a 7 Tesla superconducting magnet. Mass resolving power was m/Dm50% = 400,000 at m/z 400 (time-domain transient length was 3 seconds). Direct infusion of the samples was performed with an Advion Triversa Nanomate (Advion, Ithaca, NY). A total of 450 and 350 time-domain transients were ensemble-averaged for each sample in positive ion modes prior to fast Fourier transformation and frequency to mass-to-charge ratio conversion. Mass spectra were internally mass calibrated to provide subpart-per-million mass measurement accuracy, which facilitates direct assignment of elemental composition from the measured m/z value. Tandem mass spectrometry (collision induced dissociation, or CID) was performed for several major species observed in abundant heteroatom classes and for abundant Kendrick series thereof to correlate elemental compositions with possible molecular structures where possible. Ions of interest were isolated and fragmented to obtain MS2 and MS3 spectra; however, isolation of some peaks from the broadband mass spectra was impossible due to the high complexity of the samples and limited selection specificity of the linear ion trap CID process. Compounds were identified from MSn spectra by manual inspection and matching to reference spectra where possible.

2.6 Microbial community analysis

Genomic DNA (gDNA) was extracted from three PW and one river water samples (collected from sampling point 2 in Fig. 1a) using the DNeasy PowerWater Kit (Qiagen, Germany) according to the manufacturer's protocol. The next generation sequencing library preparations (a pool of DNA fragments with adapters attached for the Illumine sequencing platform) and Illumina MiSeq sequencing were conducted at a commercial lab (GENEWIZ, Inc., South Plainfield, NJ) to investigate the microbial community structure. The sequencing library was prepared using a MetaVx™ 16s rDNA Library Preparation kit. The samples were sequenced using a 2×250 paired-end (PE) configuration. Bioinformatics analysis was performed using a Quantitative Insights Into Microbial Ecology (QIIME2, http://qiime2.org) pipeline according to previously described methods (Wang et al., 2019). Sequences were grouped into operational taxonomic units (OTUs) using the clustering program VSEARCH (v1.9.6) against the Silva 119 database pre-clustered at a 97% sequence identity for the analysis of the microbial community taxonomic compositions.

2.7 Acute and chronic toxicity analysis

2.7.1. Acute toxicity analysis

The acute toxicity of three PW and one river water samples toward a marine luminescent bacterium *Vibrio fischeri* was measured by a Microtox® Model 500 Analyzer (Azur Environmental, DE, USA) according to the 81.9% Screening Test Protocol as described previously (Hu et al., 2020). The PW samples with different dilutions (5%, 10%, 20%, 40%, and 50% PW) were filtered through a 0.22 μm pore size membrane, and then adjusted to a pH 6~8 using solutions of 0.5 M NaOH or 0.5 M HCl prior to the toxicity test. To check the sensitivity of the luminescent bacterium *Vibrio fischeri*, $ZnSO_4$ (10 mg/L) was used as the positive control. The toxic effects were calculated based on the percentage inhibition of the luminescence intensity after 15 minutes exposure.

2.7.2. Chronic toxicity analysis

Scenedesmus obliquus and *Selenastrum capricornutum*, unicellular freshwater algae with a rapid growth rate and high sensitivity to several contaminants, were chosen for determining the chronic aquatic ecotoxicity of three PW and one river water samples. *Selenastrum*

capricornutum based chronic assay is one of the WET (Whole Effluent Toxicity) tests used by the National Pollutant Discharge Elimination System (NPDES) federal and state permitting authorities to determine whether a facility's permit and discharge complies with the WET requirements or limits. The inhibition assays were performed according to the OECD Test Guideline 201 (Oecd, 1981). The algal cultures were pre-cultured in a sterilized BG-11 medium to induce the exponential growth phase using incubators with a constant temperature of 25°C, 2800-3200 lux illumination, and a 12:12 hour light:dark photocycle. An initial cell density of 1.5×10^5 cells/mL was used in all tests. For the chronic toxicity experiments, the algal cultures were exposed to PW and river water samples with different dilutions (PW1: 20%~50%; PW2: 20%~50%; PW3: 5%~40%; river water: 50%~100%), for 10 days. The cell density was calculated using a growth standard curve based on absorbance values (at a wavelength of 680 nm) determined using a spectrophotometer (DR 6000, Hach Co., Loveland, CO). The aquatic ecotoxicity of PW was quantified based on the difference between algal cell densities in the test and control flasks during the 10-day exposure. Finally, the 10-day EC_{50} values (the concentration that results in 50% of growth rate inhibition) were established via nonlinear regression, using SPSS 13.0 software.

3. RESULTS AND DISCUSSION

3.1 Chemical characterizations of PW samples

To check data quality in this study, charge balance (or anion-cation balance) was calculated for each sample, including samples measured by the authors and samples from other sources. All the samples had a percent error lower than 10%, except for three PW samples that had errors of 10.6%, 10.4%, and 11.0%, which might be caused by sample dilution factors and analytical errors when analyzing highly saline PW samples.

Tables 1 and 2 summarize the statistical results of general water quality parameters and comprehensive element analyses (including radionuclides) of the 46 PW samples. The concentrations of TDS, TOC, and ammonia have mean values of 128,423 mg/L, 103.5 mg/L, and 432 mg/L, respectively. The results for these parameters are similar to previously reported PW quality data from the Permian Basin (Jiang et al., 2021b; Rodriguez et al., 2020). The TDS has a wide range from 100,000 to 201,000 mg/L, and the concentration of Cl^- and Na^+ (Table 2)

correspond to 62.1 % and 31.3% wt.% of the TDS. This result is consistent with previous reports that nearly all basin waters with TDS concentration above 10,000 mg/L are dominated by Na and Cl (Hanor, 1994), and that PW from the tight O&G plays is dominated by Na (median: 15,000 – 76,000 mg/L) and Cl (median: 22,000 – 150,000 mg/L) (Scanlon et al., 2020b). The median TDS in the Permian Basin (122,000 mg/L) is lower than in the Bakken tight oil (244,000 mg/L) and the Appalachian shale gas plays (166,000 mg/L), but higher than in the Eagle Ford shale play (57,000 mg/L) (Scanlon et al., 2020b).

Table 1. Statistical results of general quality parameters of the total 46 PW samples.

		Mean	Max	Min	25th percentile	50th percentile	75th percentile
Alkalinity	mg/L as $CaCO_3$	272	870	100	128	207	336
Ammonia	mg/L	432	750	320	330	400	495
COD	mg/L	1,626	3,100	930	1,250	1,400	1,950
pH	SU	6.6	8.1	3.9	6.3	6.7	7.0
TDS	mg/L	128,423	201,474	100,830	113,441	122,280	134,525
TOC	mg/L	103.5	248.1	2.4	28	90.6	173.3
TSS	mg/L	342.9	790	85	142.5	375	422.5
Turbidity	NTU	116.4	200	23	36	110	200
MBAS	mg/L	1.10	2.1	0.047	0.92	0.97	1.33

Note: COD: Chemical Oxygen Demand; TDS: Total Dissolved Solids; TOC: Total Organic Carbon; TSS: Total Suspended Solids; MBAS: Methylene Blue Active Substances.

Table 2. Statistical results of comprehensive element analyses of the 46 PW samples.

		Mean	Max	min	25th percentile	50th percentile	75th percentile
Cations							
Aluminum	mg/L	1.09	3.95	0.37	0.63	0.76	1.25
Arsenic	mg/L	3.17	6.04	1.62	1.74	2.64	4.61
Barium	mg/L	2.21	12.00	0.10	0.45	1.69	3.00
Beryllium	mg/L	0.03	0.04	0.01	0.01	0.03	0.04
Bismuth	mg/L	1.02	1.77	0.71	0.72	0.81	1.55
Boron	mg/L	42.34	76.50	17.20	33.29	40.65	51.03
Cadmium	mg/L	0.47	0.81	0.04	0.08	0.63	0.77
Calcium	mg/L	3,821	8,186	880	1,705	3,531	5,744
Chromium	μg/L	1.69	2.19	1.31	1.31	1.57	2.19
Cobalt	μg/L	7.66	7.84	7.47	7.47	7.68	7.84
Copper	mg/L	0.65	1.46	0.24	0.24	0.45	1.26
Ferrous iron	mg/L	3.09	6.70	0.57	0.73	3.00	5.50
Iron	mg/L	19.35	65.20	0.50	4.60	14.00	25.70
Lithium	mg/L	22.39	52.28	11.74	20.00	21.02	23.40
Magnesium	mg/L	745.0	1,877	295.3	472.7	621.3	959.1
Manganese	μg/L	488.5	1,239	10.0	116.0	426.5	780.8
Molybdenum	mg/L	0.21	0.38	0.10	0.11	0.18	0.35
Potassium	mg/L	923	3,637	222	449	808	1,171
Selenium	mg/L	2.5	2.5	2.5	n/a	2.5	n/a
Silica	mg/L	107.7	195.4	4.0	29.2	115.7	178.2
Sodium	mg/L	40,896	68,985	25,080	37,000	39,673	42,967
Strontium	mg/L	449.9	1,404	28.9	116.4	325.3	816.5
Thallium	mg/L	0.83	0.84	0.82	n/a	0.83	n/a
Vanadium	μg/L	79.63	94.51	61.39	61.39	82.98	94.51
Zinc	mg/L	1.14	1.81	0.17	0.17	1.45	1.81
Anions							
Sulfate	mg/L	496	965	151	243	510	690
Phosphorus	mg/L	8.5	36.0	1.7	2.5	6.4	8.9
Nitrite as N	mg/L	n/a	16	n/a	n/a	n/a	n/a
Iodide	mg/L	88	94	77	82	90	94
Chloride	mg/L	78,648	120,200	57,543	69,269	75,658	86,979
Bromide	mg/L	431	960	95	238	289	608
Radionuclides							
Gross Alpha	pCi/L	1,105.6	1,630	660	745	863	1,630
Gross Beta	pCi/L	874.6	1,230	456	748	889	1,050
Radium-226	pCi/L	43.92	111	0.74	13.9	22.4	72.75
Radium-228	pCi/L	151.3	291	2.56	35.9	153	273

Note: n/a: not available.

TDS provides an indication of the PW mineral content, which is a major concern for PW management, treatment, and reuse. High salinity water corrodes metal pipes and tanks, which causes problems for PW transport, storage, and treatment. In addition, high concentrations of scale-forming ions, such as Ca^{2+} (mean concentration of 3,821 mg/L), Mg^{2+} (745 mg/L), Sr^{2+} (450 mg/L), SO_4^{2-} (496 mg/L), and SiO_2 (108 mg/L), can cause severe scaling and decrease the performance of the management/treatment system. The SO_4^{2-} ion can also be reduced to H_2S by sulfate-reducing bacteria, which is a safety hazard to workers in addition to being extremely corrosive.

High TDS also affects the choice of treatment methods. Reverse osmosis (RO) usually can treat water with TDS < 30,000 – 45,000 mg/L. For unconventional PW with higher TDS concentration found across the Permian Basin, thermal techniques are required for treatment, such as thermal distillation and solar still (Chen et al., 2021; Liden et al., 2019; Liden et al., 2018). Resource and mineral recovery from PW has also been reported in a previous study which simultaneously recovered NH_4^+, K^+, and Mg^{2+} from PW by struvite precipitation after calcium pretreatment (Hu et al., 2021). Following mineral recovery, softened PW can be further treated for different fit-for-purpose applications.

PW usually contains NORM, with the high concentration of Cl^- enhancing the solubility of NORM (Fisher, 1998). Currently, there is very little data or other information regarding NORM in Permian Basin PW. Nine of the PW temporal samples were analyzed for NORM. Ra-226 (half-life of 1,500 years) and Ra-228 (half-life of 5.75 years) were chosen because they are the most abundant (Burden et al., 2016). The results show the total Ra (Ra-226 + Ra-228) has an average level of 195 pCi/L (pico-curies/L), which is much higher than the EPA regulatory limit of 5 pCi/L for drinking water. The results in this study are lower in comparison to another study for the Permian Basin (535 pCi/L) and lower than other major O&G production basins; Marcellus shale (median: 1,980 pCi/L), Bakken (1,200 pCi/L), and the maximum is close to Eagle Ford (284 pCi/L) (Scanlon et al., 2020b). Also, the results show a large temporal variance between the PW samples, from 2.56 to 291 pCi/L for Ra-228 and from 0.74 to 111 pCi/L for Ra-226.

PW may contain naturally occurring radioactive material (NORM), and the high concentration of Cl^- enhances the solubility of NORM (Fisher, 1998). Currently, there is limited

data or information regarding the presence of NORM in Permian Basin PW. The ten PW temporal samples collected from Sampling Point 2 (Fig. 1a) were analyzed for NORM. Radium-226+228, uranium-234+238, thorium-228+230, polonium-210, and plutonium-238 were detected in the samples. In contrast, neptunium-237, americium-241, uranium-235, thorium-232, and plutonium-239+240 were not detected. Ra-226 (half-lives of 1,600 yr) and Ra-228 (half-lives of 5.75 yr) were chosen for comparison because they are the most abundant and most widely detected in other basins and represent the first soluble daughter product in the uranium-238 and thorium-232 decay chains, respectively. Results show total Ra (Ra-226 + Ra-228) has a mean level of 469.3 pCi/L (pico curies/L). As references, the results in this study are similar to a previous study for the Permian Basin (535 pCi/L), lower than other major O&G production basins such as Marcellus shale (median: 1,980 pCi/L) and Bakken (1,200 pCi/L), and higher than Eagle Ford (284 pCi/L) (Scanlon et al., 2020b). These results also show a large temporal variance between PW samples from 2.56 to 576 pCi/L for Ra-228 and from 0.74 to 970 pCi/L for Ra-226 in Sampling Point 2.

While the focus is primarily on the quantitation of Ra-226 and Ra-228, both exist as parts of the uranium-238 and thorium-232 decay chains, respectively. Parent and daughter isotopes have been identified in PW, although the various long-lived parent products (e.g., thorium-230 and thorium-228, respectively) are largely insoluble and both decay into gases (radon-222 and radon-224), which can be transported elsewhere.

3.2 Dissolved organic matter in PW characterized by FEEM analyses

It is costly and time-consuming to analyze the whole profile of organic compounds in PW samples because they contain numerous anthropogenic and natural organics. 3D-FEEM can provide pragmatic information for the dissolved organic matter (DOM) in PW based on the phenomenon that a large portion of organic compounds, such as proteins and bacterial metabolites (fulvic and humic substances), have fluorescent emission characteristics (Jiang et al., 2021a). Although FEEM lacks quantitative information on specific compounds, it provides low cost and real-time results compared to GC/LC-MS, and the advantages of higher selectivity and a wider range compared to conventional fluorescence.

In this study, FEEM was used to characterize DOM in three PW samples from the Delaware Basin and one Pecos River sample from Carlsbad, NM (Fig. 2). All three PW samples have similar peaks in regions I, II, III, and IV. However, intensities varied between peaks. PW3 has more peaks compared to PW1 and PW2. PW1 and PW2 have the strongest peaks in region IV, indicating a high concentration of microbial byproduct-like materials associated with the activity of microbial metabolism. If these PWs are to be reused for HF, more biocides may be required. PW3 has the strongest peak in regions I, II, III, and IV that represent high concentrations of aromatic carbon, fulvic acid-like compounds, and microbial byproduct-like materials (Dahm et al., 2013). PW1 and PW2 showed relatively lower peak intensity in region III, fulvic acid-like compounds. All samples had low-intensity peaks in region V, which are humic acid-like material. Such quick FEEM analyses could be performed in a field lab as a real-time indicator of organic substances and petroleum hydrocarbons to assist in on-site evaluation of PW treatment performance. The Pecos River sample showed much lower intensity (0 - 0.025) of DOM compared with PW samples (0 - 0.7). The major peaks for the Pecos River sample represent aromatic carbon (regions I and II) and fulvic acid-like compounds (region III).

The FEEM results, however, do not provide more information regarding the specific organic compounds and their quantity. Some compounds may cause negative environmental and health impacts in very low concentrations. Thus, targeted organic compound analyses were performed in this study to investigate the organic profile in PW samples.

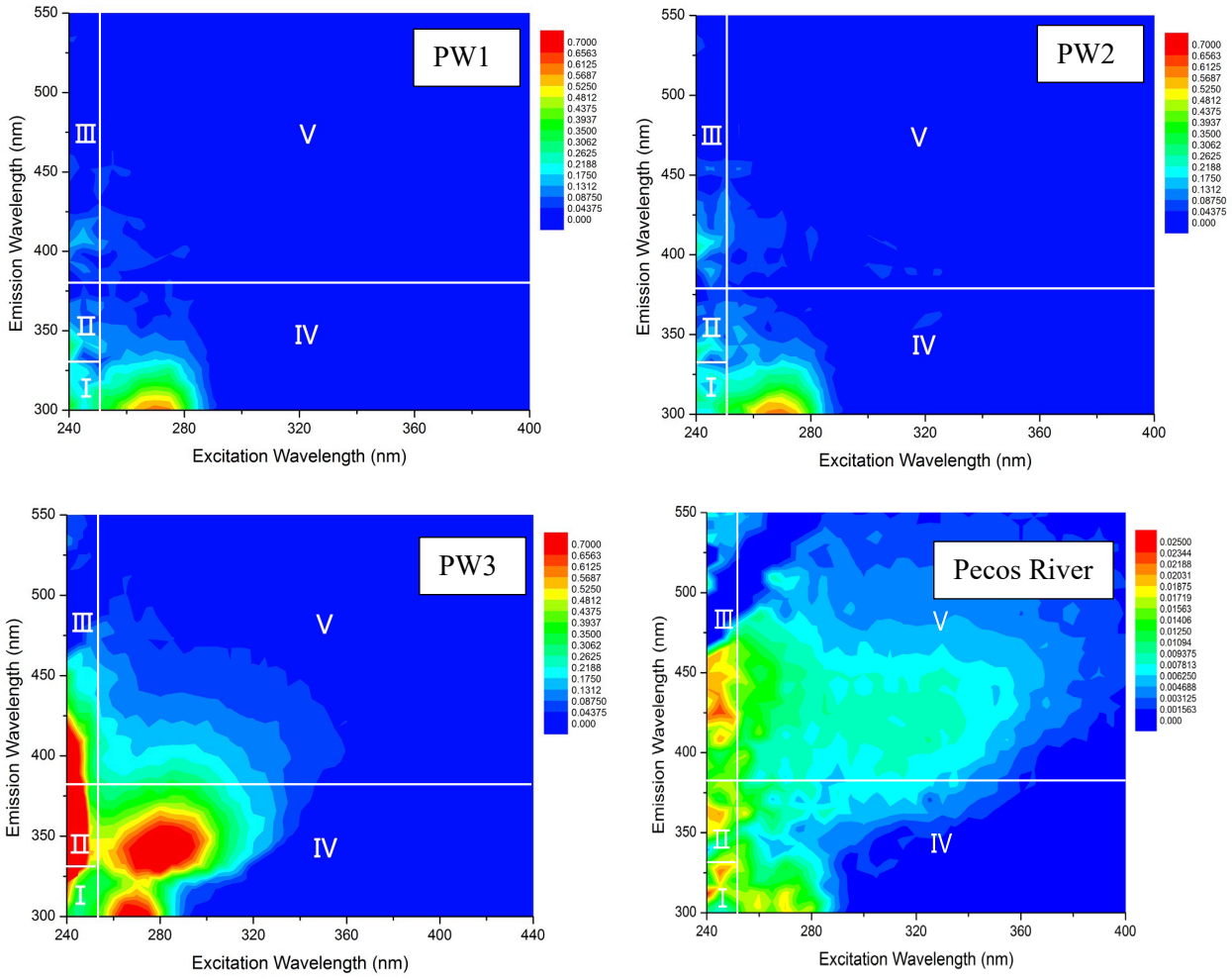

Fig. 2. FEEM spectra of three PW samples from the Delaware Basin and one Pecos River sample from Carlsbad, New Mexico. All spectra are normalized to 1 mg/L DOC with a suitable scale for fluorescence intensity (PW: 0 - 0.7; Pecos River: 0 - 0.025).

3.3 Targeted organic analyses

Advanced analytical instruments/methods were used for the targeted analysis of organic compounds in the ten temporal PW samples (NM-PW from Sampling Point 2 in Fig. 1a). In summary, 28 organic compounds (not including diesel range organics (DRO), gasoline range organics (GRO), and motor oil range organics (MRO)) were quantitatively identified in the PW samples (Table 3), while other 221 other constituents were not detected. The list of undetected compounds can be found in Appendix Table A1.

Table 3. Statistical results of the detected organic compounds in ten PW samples.

		Mean	Max	Min	25th percentile	50th percentile	75th percentile
VOC							
Benzene	µg/L	2,611.1	4,900	1,900	2,200	2,200	2,600
Ethylbenzene	µg/L	112.22	160	72	93	110	130
Toluene	µg/L	2,533	3,700	1,700	2,000	2,400	2,900
Xylenes, Total	µg/L	1,185.6	1,600	710	1,100	1,300	1,400
SVOC - General							
1,1'-Biphenyl	µg/L	5.89	8.5	3.8	4.6	5.2	7.2
1,4-Dioxane	µg/L	n/a	21	ND	n/a	n/a	n/a
1-Methylnaphthalene	µg/L	22.67	36	15	18	21	26
2-Methylnaphthalene	µg/L	38.33	65	26	29	36	45
2-Methylphenol	µg/L	81.78	98	68	77	80	85
2,4-Dimethylphenol	µg/L	34.14	42	29	31.5	33	36
Ethylene glycol	mg/L	n/a	27	ND	n/a	27	n/a
Ethanol	mg/L	0.51	0.98	0.14	0.21	0.57	0.67
Methanol	mg/L	24.52	52	5.6	12	26	27
Methylphenol, 3 & 4	µg/L	90.44	110	72	85	91	96
Phenol	µg/L	203.33	250	170	170	210	220
Pyridine	µg/L	237.5	300	120	235	240	260
Pesticides/Herbicides							
alpha-BHC	µg/L	0.018	0.027	0.0088	n/a	n/a	n/a
Endosulfan I	µg/L	0.855	0.98	0.73	n/a	n/a	n/a
Endrin	µg/L	n/a	0.0038	ND	n/a	0.0038	n/a
Organic Acids							
Acetic acid	mg/L	n/a	89	n/a	n/a	n/a	n/a
Butyric acid	mg/L	n/a	7.1	n/a	n/a	7.1	n/a
Propionic acid	mg/L	n/a	5.7	n/a	n/a	5.7	n/a
SVOC-PAH							
Anthracene	µg/L	n/a	1.1	ND	n/a	n/a	n/a
Naphthalene	µg/L	15.44	24	11	12	16	16
Phenanthrene	µg/L	3.76	6.6	2.7	3.18	3.4	4.03
Fluorene	µg/L	4.35	5.6	3.1	n/a	4.7	n/a
Carbonyl Compounds							
Formaldehyde	mg/L	0.14	0.21	0.053	0.11	0.15	0.18
SVOC-TPH							
n-Decane	µg/L	556.7	890	340	390	530	610
Oil and Grease							
DRO (C10-C20)	mg/L	49	130	22	26	35	52
GRO (C6 - C10)	mg/L	23.5	46	13	15	19.5	28
MRO (C20-C34)	mg/L	32.44	97	12	16	26	32
Tributyl phosphate	µg/L	34.6	74	3.3	12	30.5	53
Tentatively Identified Compound	µg/L	531.1	1,000	280	320	350	840

Note: n/a: data not available; ND: not detected. PAH: Polycyclic aromatic hydrocarbon; TPH: Total petroleum hydrocarbons; DRO: Diesel Range Organics; GRO: Gasoline Range Organics; MRO: Motor oil Range Organics.

Table 3 shows the statistical results of organic compounds quantified during the analyses of the ten PW-NM samples. Detected VOCs include benzene (min – max: 1,900 – 4,900 µg/L), toluene (1,700 – 3,700 µg/L), ethylbenzene (72 – 160 µg/L), and xylene (710 – 1,600 µg/L, BTEX), of which benzene, toluene, and xylene had the highest relative abundances. Results are consistent with other studies and are anticipated because these compounds are closely related to O&G production (Lester et al., 2015). BTEX constituents usually have the highest concentrations during the flowback period (Luek and Gonsior, 2017). No other VOCs were detected, which may be because samples were collected at a SWD site, and volatilization might occur during transportation and storage before sampling. For general SVOCs, phenol (170 – 250 µg/L) and pyridine (120 – 300 µg/L) have the highest relative abundances. Phenol has been reported as being used in HF fluid to help coat sand proppants and as a disinfectant to eliminate bacteria (Jackson, 2014). The leaching of phenol and formaldehyde (also detected in this study) depends on the temperature in the formation (Mazerov, 2013; Schenk et al., 2019). Pyridine is the most frequently detected SVOC in HF fluids, which may be due to its use as a precursor for one of the HF additives (U.S. EPA, 2011), and it has been reported as naturally occurring in oil shales (Roper, 1992). Alcohols are also used for several functions in HF fluids, production chemistry, and SWD treatment chemistry. They are routinely used as solvents, surfactants, gelling agents, friction reducer, and corrosion inhibitors. Mostly frequently used alcohols include methanol (5.6 – 52 mg/L), ethanol (0.14 – 0.98 mg/L), ethylene glycol (ND – 27 mg/L), and phenols (FracFocus, 2021). Different alcohols were detected in this study; however, they are likely from production and SWD treatment chemistry, not HF chemistry. Other SVOCs such as 1,4-Dioxane (ND – 21 µg/L), 1-Methylnaphthalene (15 – 36 µg/L), and 2,4-Dimethylphenol (29 – 42 µg/L) were detected in this study and reported in other studies (Luek and Gonsior, 2017).

Biocides are often added to HF fluids and fluids associated with production operation for unconventional O&G development and SWD treatment to inactivate bacteria that are ubiquitous in the environment and cause problems during HF, including biofouling, production of toxic H_2S, and corrosion of metal equipment (Jiang et al., 2021a). In this study, the commonly used biocides, including quaternary ammonium chloride and glutaraldehyde for HF, were not detected (FracFocus, 2021). Detected biocides were in very low concentrations: alpha-BHC (0.009 – 0.027 µg/L), endosulfan I (0.73 – 0.98 µg/L), and endrin (ND – 0.004 µg/L). Reasons for these results may include, firstly, the biocides can react with microbes and other chemicals during the

HF and be degraded to other organic compounds. Secondly, biocides can undergo chemical changes in the subsurface, which has different temperatures, salinity, and pH. A study simulated the transformation of glutaraldehyde during HF and found that the fate of glutaraldehyde depended on downhole conditions. It can undergo rapid auto-polymerization and sorb onto shale and then remain underground, or it can remain stable and return to the surface with a half-life of 20 days (Kahrilas et al., 2016). Thirdly, samples collected in this study were mainly PW, in which biocides may have a lower concentration than in HF flowback water.

Acids are used as iron controllers and pH adjusting agents during O&G production. A relatively high concentration of acetic acid (max: 89 mg/L) was detected in this study; two other acids (butyric acid: 7.1 mg/L and propionic acid: 5.7 mg/L) with lower concentrations were also detected. They may correspond with SWD treatment chemistry. However, it may also come from anaerobic microbial metabolism by degrading the biopolymers during the HF (Olsson et al., 2013) or degradation of organic matter in the reservoir at temperatures above 80°C (Carothers and Kharaka, 1978). Better control of bacteria in PW may decrease its concentrations.

Polycyclic aromatic hydrocarbons (PAHs) are a large class of cancer-causing chemicals and occur naturally in coal, crude oil, and gasoline. They have been quantitatively reported in several studies, including in Denver-Julesburg Basin flowback samples (Lester et al., 2015) and in Marcellus PW samples (Jackson, 2014). According to the United States Centers for Disease Control and Prevention, the health effects of people exposed to low levels of PAHs are unknown; large amounts of PAHs can cause blood and liver abnormalities (Centers for Disease Control and Prevention, 2019). The detected PAHs in this study include anthracene (min – max: ND – 1.1 µg/L), naphthalene (11 – 24 µg/L), phenanthrene (2.7 – 6.6 µg/L), and fluorene (3.1 – 5.6 µg/L). As anticipated for PW samples, DRO (22 – 130 mg/L), GRO (13 – 46 mg/L), and MRO (12 – 97 mg/L) were detected in relatively high concentrations.

A mean of 531 µg/L tentatively identified compounds (TICs) were detected in the PW samples. TIC refers to a compound that can be detected by the analysis method, but its identity cannot be confirmed without further investigation. All VOC and SVOC samples analyzed by the commercial laboratory were subject to TIC searches using the National Institute of Standards and Technology (NIST) mass spectra library, which consists of hundreds of thousands of identified compounds. To improve hazard and risk assessment, and reduce concern for reuse of treated PW,

an effort should be made to identify compounds of concern within this unresolved fraction (U.S. EPA, 2020). A TIC can be converted to a target analyte if the method is developed to include the compound. This can be done by including reference standards for the chemical in calibration and quality control samples. Our future research will focus on the non-target analysis of these unknown chemicals in raw/untreated and treated PW using high-resolution LC/MS.

3.4 Non-targeted organic analyses

Data Analysis

The complex mixture analysis data for each of the samples was generated through FT-ICR-MS chemical analysis. Double Bond Equivalence (DBE) was used to characterize the data, and DBE represents the number of rings plus the number of double bonds in a given molecular formula. DBE values can be calculated by the following equation:

$$DBE = c-(h/2)+(n/2)+1$$

where c, h, n are the number of carbon, hydrogen or halogen, and nitrogen respectively for an individual compound's formula for elemental formulas of the type $C_cH_hN_nO_oS_s$ (Cho et al., 2013). Additionally, Van Krevelen Diagrams were used, which are a plot of the oxygen to carbon atomic ratio versus the hydrogen to carbon atomic ratio.

Fig. 3 presents cross-plots of DBE as a function of carbon number to reveal the complexity and diversity of PWs composition (samples 1 and 2), river water (sample 3), groundwater (sample 5, and drinking water (sample 6). In shale oil from the Permian Basin, compounds with DBE values between 4 and 7 (analyzed by FT-ICR-MS with +APPI) are the more abundant compounds, which have mono or bicyclic aromatic structures (Cho et al., 2013). This research found that the Permian Basin PWs also have dominant organic compounds with DBE values ranging from 3 to 7 (Fig. 3). Higher DBE values are indicative of greater aromaticity and less saturation. It is also interesting to compare organic characteristics of PW with organic characteristics of river water, groundwater, and drinking water from the Permian Basin. Asphaltenes are typical constituents of petroleum that have DBE values generally higher (20 – 35) than byproducts of petroleum such as PWs (Wang et al., 2012), which is also similar to the results for shale oil (Jin et al., 2012). This research observed lower DBE (0-6) for asphaltenes in PW, river water, groundwater, and drinking water from the Permian Basin, which is also in

agreement with previous work (Wang et al., 2012). The trends shown for the various PW samples are not significantly different from each other (Fig. 3). The most abundant compounds are present at DBE= 3-7, and Carbon number = 25-35.

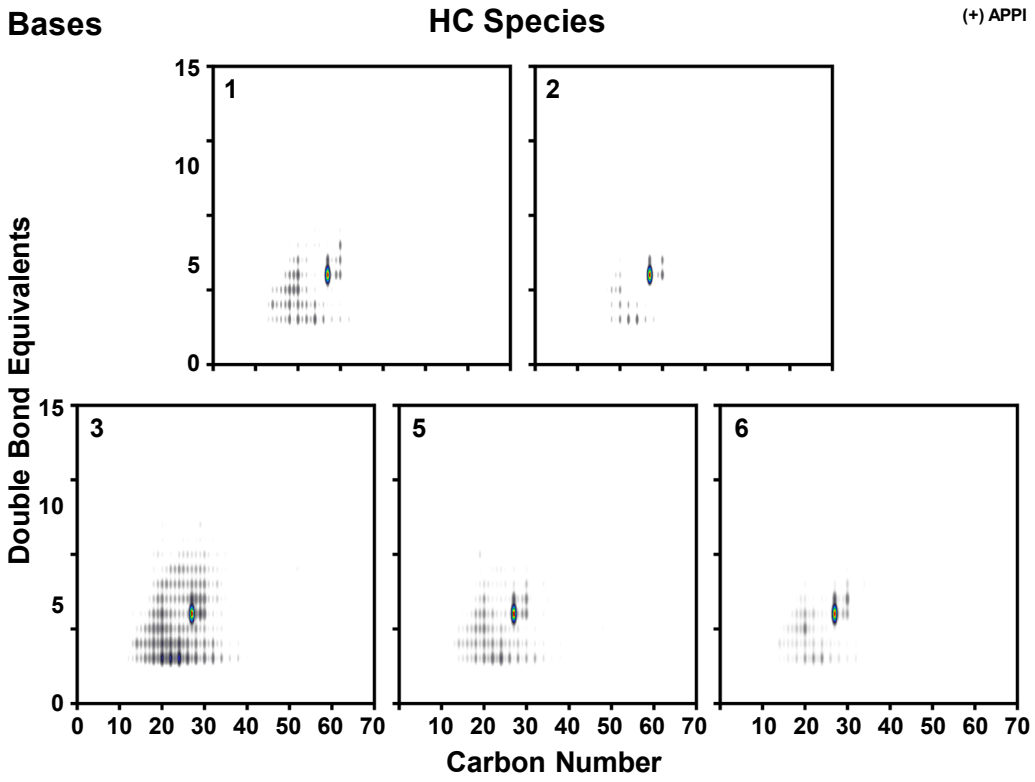

Fig. 3. 3-D Contour plots for double-bond equivalent (DBE) versus carbon (C) number relative abundance illustrating similar trends among the samples. DBE or double bond equivalent measure the level of unsaturation, or the number of unsaturations present in an organic molecule. The term "unsaturation" means a double bond or a ring system.

Fig. 4 presents the 2-D Van Krevelen diagram characterization of samples collected for this study. According to Fig. 4 (which is the key to interpreting a Van Krevelen diagram), organic compounds in PW are characterized as both Type I (Lacustrine) and Type II (Marine) sources, which is supported by the geologic history of the Permian Basin and its sedimentary rock formations. Fig. 4 also shows that diagenesis altered the composition of the organics within PW samples, as well as river water, groundwater, and drinking water (source of drinking water is groundwater), which was expected only for the PW sample results. Despite the significant difference in concentrations (which is not considered for this report except in Fig. 2), the distribution of structures is similar for the PW and the freshwater samples.

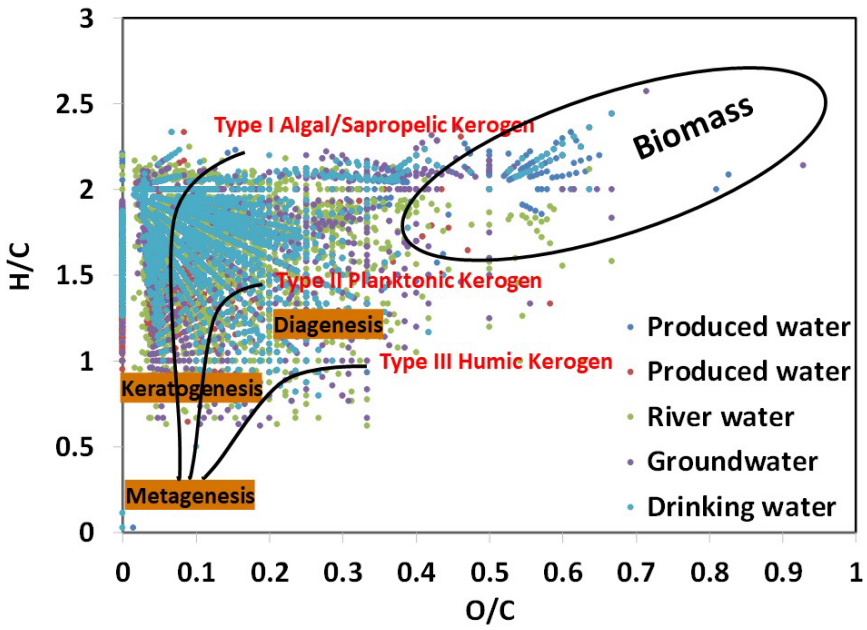

Fig. 4. Conceptual diagram of the 2-D Van Krevelen Diagram with data from the present study.

There are generally three main categories or types used to characterize the evolution of organic materials, as identified in Fig. 4. A summary of the three types is useful for evaluating the processes impacting organic matter composition variability. Type I: (Sapropelic) Deposition of algae in anoxic conditions is the process of forming Type I kerogen. Lacustrine algae has great affinity to form liquid hydrocarbons such as crude oil or shale oil because of its elevated percentage of lipids in it relative to terrestrial plants. Type II: (Planktonic) Type I has less oxygen than Type II, and Type II is more favorable for producing Plankton in marine settings as the main source for creating a mixture of gas and oil. For Type II kerogens, organic materials are deposited in a reduced environment rather than in purely anoxic conditions like Type I kerogen.

Type II kerogens also have increased sulfur content. Type III: (Humic) Wood, leaves, and other fibrous materials from terrestrial plants are the main sources for composing this category. As terrestrial plants are lowest in lipid concentration as well as deficient in the required amount of hydrogen to form hydrocarbon chains, Type III is feasible for producing coal and gas. Type III can create liquid hydrocarbons only for very specific conditions. Fig. 4 confirms that the samples were mainly characterized as Type I and II with a minor amount of Type III.

The 2-D Van Krevelen diagrams in Fig. 5 depict the mass spectra of heteroatoms (any atoms other than carbon or hydrogen such as N, O) in PW samples collected from storage pond/tanks, river water, groundwater, and drinking water from the Permian Basin. Although the highest relative abundance was observed at H/C = 1.5 - 2.3, O/C = 0.07-0.26 and H/C = 0.83 – 1.2, O/C = 0.08 - 0.15 for PW samples, the clusters of compounds (meaning the place in the Van Krevelen Diagram where most compounds are located) among different samples did not show similar trends between samples of different water types. In the river water samples, there were also no distinct trends observed. Whereas, for the groundwater in Fig. 4 there was a similar trend for H/C and O/C ratios compared to the PW (Well 2) samples. Through comparison of the PW samples in Fig. 5, the Well 1 sample showed only a decreasing trend for H/C and O/C ratios, whereas Well 2 had both increasing and decreasing trends. Also, the PW from Well 1 had more biomass compounds (such as humic acids) compared to PW from Well 2.

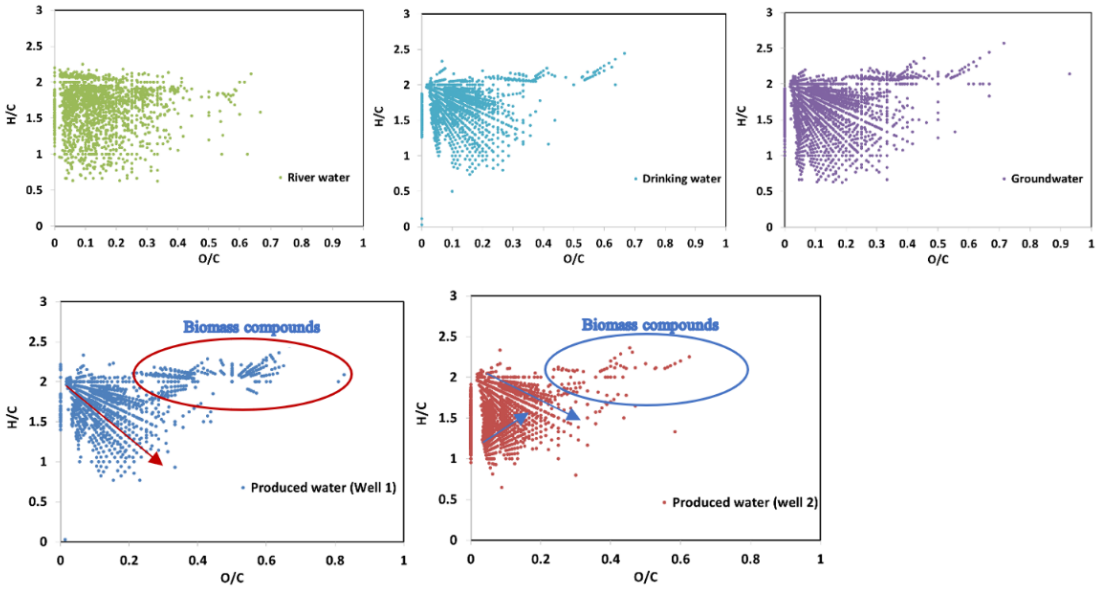

Fig. 5. 2-D Van Krevelen (H/C vs O/C) diagram for PW, river water, groundwater, and drinking water samples illustrating the fingerprints of hetero-hydrocarbons present in those samples.

3.5 Microbial community analysis

The bacterial community structures in PW and river water samples were analyzed using Illumina MiSeq^{TM} high-throughput sequencing technology. Fig. 6 presents the taxonomic compositions (phylum, class, order, family, and genus levels) of bacterial communities. Three PW samples showed a similar bacterial community structure. At the phylum level (Fig. 6a), the most abundant phyla in PW samples were *Proteobacteria* (57.5%~67.2%) and *Firmicutes* (28.6%~37.1%), which were also generally detected as the abundant bacterial phyla in other flowback and PW samples (Huang et al., 2020; Wang et al., 2019). *Gammaproteobacteria* and *Clostridia* were the predominant classes in PW with the relative abundances of 50.0%~59.3% and 23.6%~36.5%, respectively (Fig. 6b). At the order level (Fig. 6c), *Alteromonadales* (31.6%~54.0%) and *Halanaerobiales* (23.6%~36.4%) dominated the bacterial community in PW samples. At the family level (Fig. 6d), the relative distribution of taxonomic groups in PW exhibited a similar pattern, in which *Alteromonadaceae* and *Halanaerobiaceae* contributed more than 60% of the bacteria in all PW samples. Among the top 15 predominant genera (Fig. 6e), *Marinobacter* (30.9%~54.0%) and *Halanaerobium* (23.3%~36.3%) were dominant in all PW samples. *Marinobacter* has been widely detected in petroleum-contaminated environments and regarded as an active PAHs degrader in saline environments (Wang et al., 2020). *Halanaerobium* was found to be the most abundant organism in the majority of the PW samples and has a critical role in hydraulic fracturing-related microbial activity (Lipus et al., 2017). Some *Halanaerobium* sp. strains have the potential for acid production, thiosulfate reduction, and biofilm formation, suggesting an ability to contribute to pipeline corrosion, souring, and biofouling events in hydraulic fracturing infrastructure (Liang et al., 2016). The highest abundance of *Halanaerobium* in PW1 suggests it may cause the most sever corrosion compared with other PW samples.

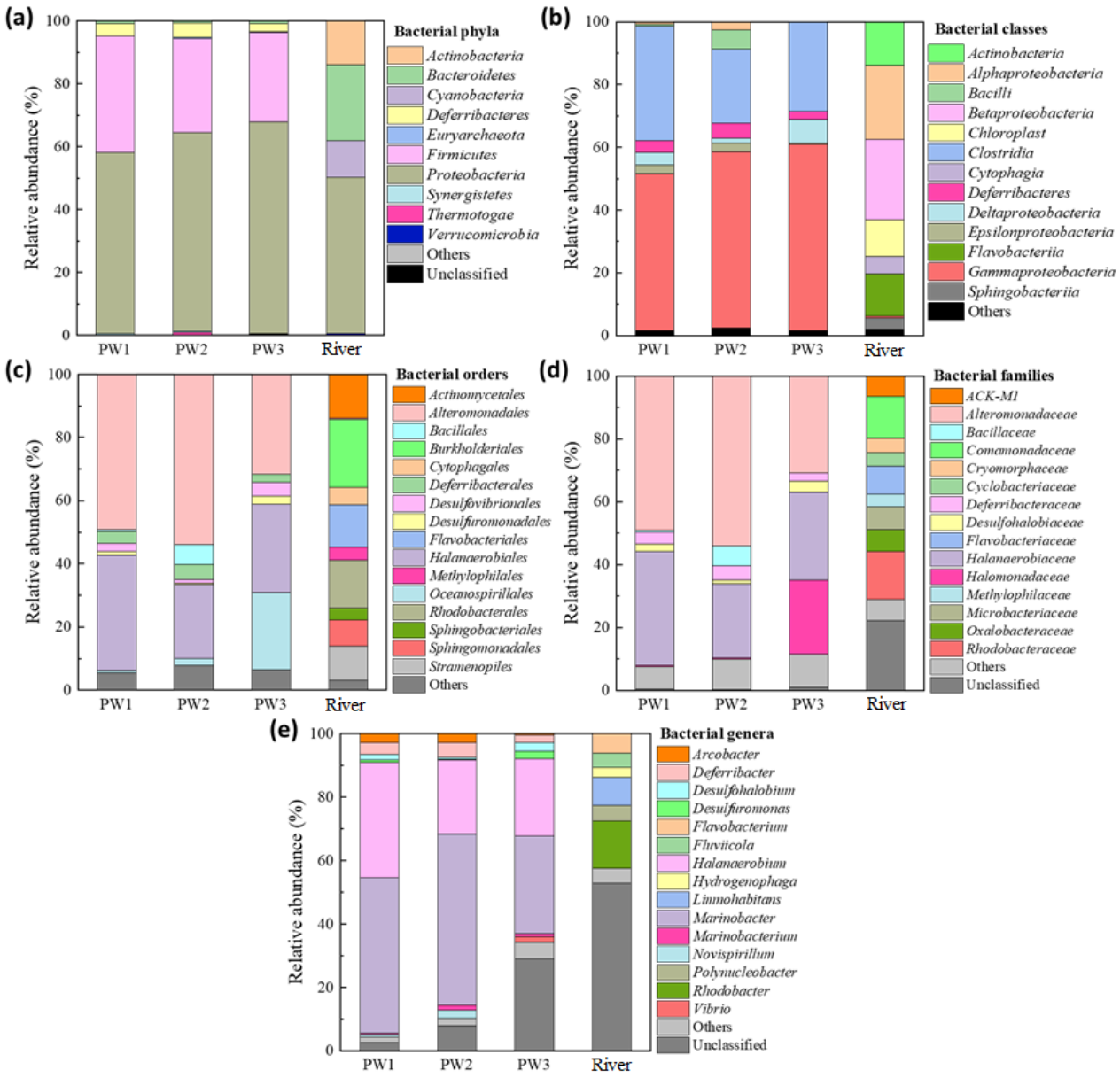

Fig. 6. Relative abundance of major taxonomic groups at the (a) phylum, (b) class, (c) order, (d) family, and (e) genus level in different PW and river water samples. Contributors with abundance less than 1% in all libraries are termed as "Others".

Bacterial community structure of river water was drastically different from that in PW. *Proteobacteria* (49.7%), *Betaproteobacteria* (25.5%), *Burkholderiales* (21.5%), *Rhodobacteraceae* (15.2%), and *Rhodobacter* (15.0%) were the most abundant phylum, class, order, family, and genus in river water, respectively.

3.6 Acute and chronic toxicity

The high salinity of PW was considered as a major mechanistic mode of toxicity for exposed organisms (He et al., 2017). In addition, other potentially harmful chemical species present in PW, including organic petroleum-related hydrocarbon species (e.g., PAHs), heavy metals (lead, arsenic, nickel), radionuclides, and industrial fracturing additives such as biocides, surfactants, and polymers, may also contribute to the whole toxicity of PW (Folkerts et al., 2017). Thus, to properly assess risk, having an *a priori* understanding of the ecotoxicity effects of PW to different organisms is necessary for both risk management and in helping to define the most toxic components and necessary treatment strategies prior to PW discharge and reuse.

3.6.1. Acute toxicity

The levels of *Vibrio fischeri* bioluminescence inhibition after 15 minutes of exposure to PW with different dilution times are shown in Fig. 7. The inhibition of the luminescence intensity after 15 minutes exposure was very low (less than 10%) when *Vibrio fischeri* was exposed to 5%~10% PW. However, when *Vibrio fischeri* was exposed to 40%~50% PW, the percentage bioluminescence inhibition of all PW samples significantly increased to 81%~99%. In contrast, there was no adverse effect observed when *Vibrio fischeri* was exposed to river water. The *in vitro* toxicity is commonly demonstrated based on the EC_{50} value, which is the concentration causing 50% inhibition of a specific biological or biochemical function. In this work, the EC_{50} of PW1, PW2, and PW3 for *Vibrio fischeri* were 23.2%, 29.6%, and 24.5%, respectively (Table 4).

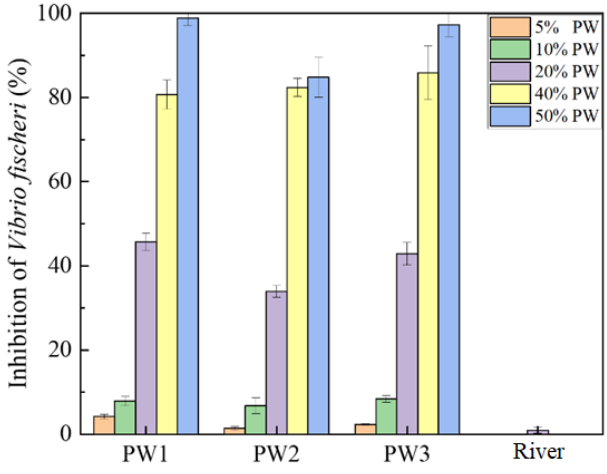

Fig. 7. The toxic effect of PW and river water samples on *Vibrio fischeri* bioluminescence after 15 minutes of exposure.

Table 4. Results of direct toxicity assessment of PW using three different test organisms.

Organisms	Exposure time	Endpoint	EC_{50}		
			PW1	PW2	PW3
Vibrio fischeri (luminescent bacterium)	15 min	Acute	23.2%	29.6%	24.5%
Scenedesmus obliquus (freshwater algae)	10 d	Chronic	26.7%	30.9%	8.1%
Selenastrum capricornutum (freshwater algae)	10 d	Chronic	19.2%	36.4%	14.7%

3.6.2. Chronic toxicity

Growth inhibition of *Scenedesmus obliquus* and *Selenastrum capricornutum* after the 10 days of exposure to PW with different dilutions are shown in Figs. 8 and 9, respectively. PW1 showed 78.7% and 88.6% of algal growth inhibition after 10 days when *Scenedesmus obliquus* was exposed to 40% and 50% PW1, respectively (Fig. 8a). 10-day inhibition of an algal population was 76.7% and 81.8% after incubation with 40% and 50% PW2 (Fig. 8b), respectively. However, 20% PW3 showed a significantly high inhibition (90.9%) on the growth of *Scenedesmus obliquus*, which was much higher than that in 20% PW1 (42.9%) and 20% PW2 (40.9%), indicating PW3 should be more toxic than PW1 and PW2 for freshwater algae. The chronic toxicity experiments based on *Selenastrum capricornutum* (Fig. 9) showed similar results to *Scenedesmus obliquus*. In contrast, as presented in Figs. 8d and 9d, river water could promote algae growth, which may be ascribed to high nitrogen concentration in river water. Table 4 presents the EC_{50} values of PW1, PW2, and PW3 for *Scenedesmus obliquus* and *Selenastrum capricornutum*. In this work, the EC_{50} values of PW1, PW2, and PW3 for *Scenedesmus obliquus* were 26.7%, 30.9%, and 8.1%, respectively. The EC_{50} values of PW1, PW2, and PW3 for *Selenastrum capricornutum* were 19.2%, 36.4%, and 14.7%, respectively. Thus, the chronic toxicity of the three PW samples was ranked as PW3 > PW1 > PW2.

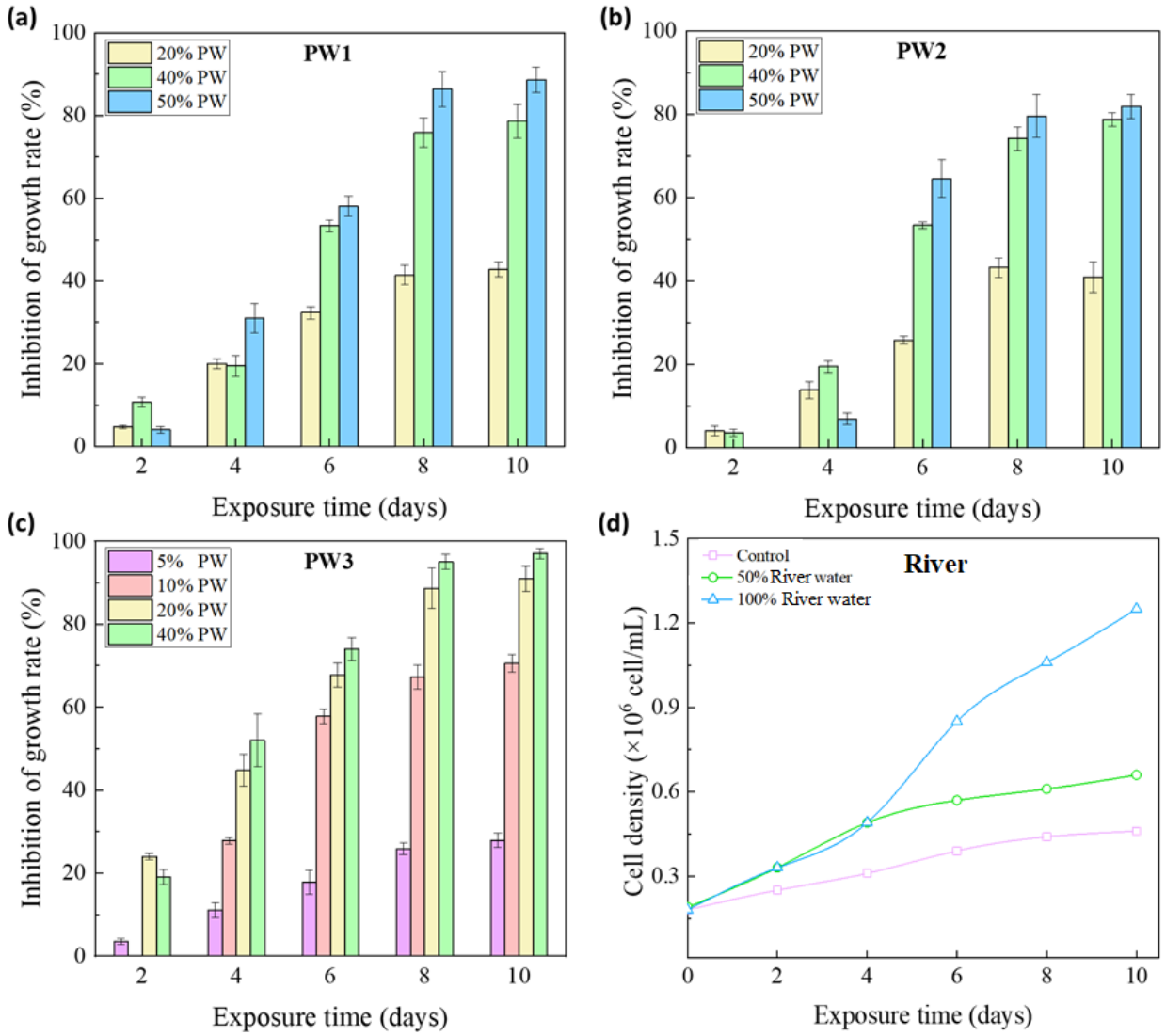

Fig. 8. Growth inhibition rate of *Scenedesmus obliquus* during 10-day exposure to different PW samples: (a) PW1, (b) PW2, (c) PW3; (d) growth curve of *Scenedesmus obliquus* during 10-day exposure to river water.

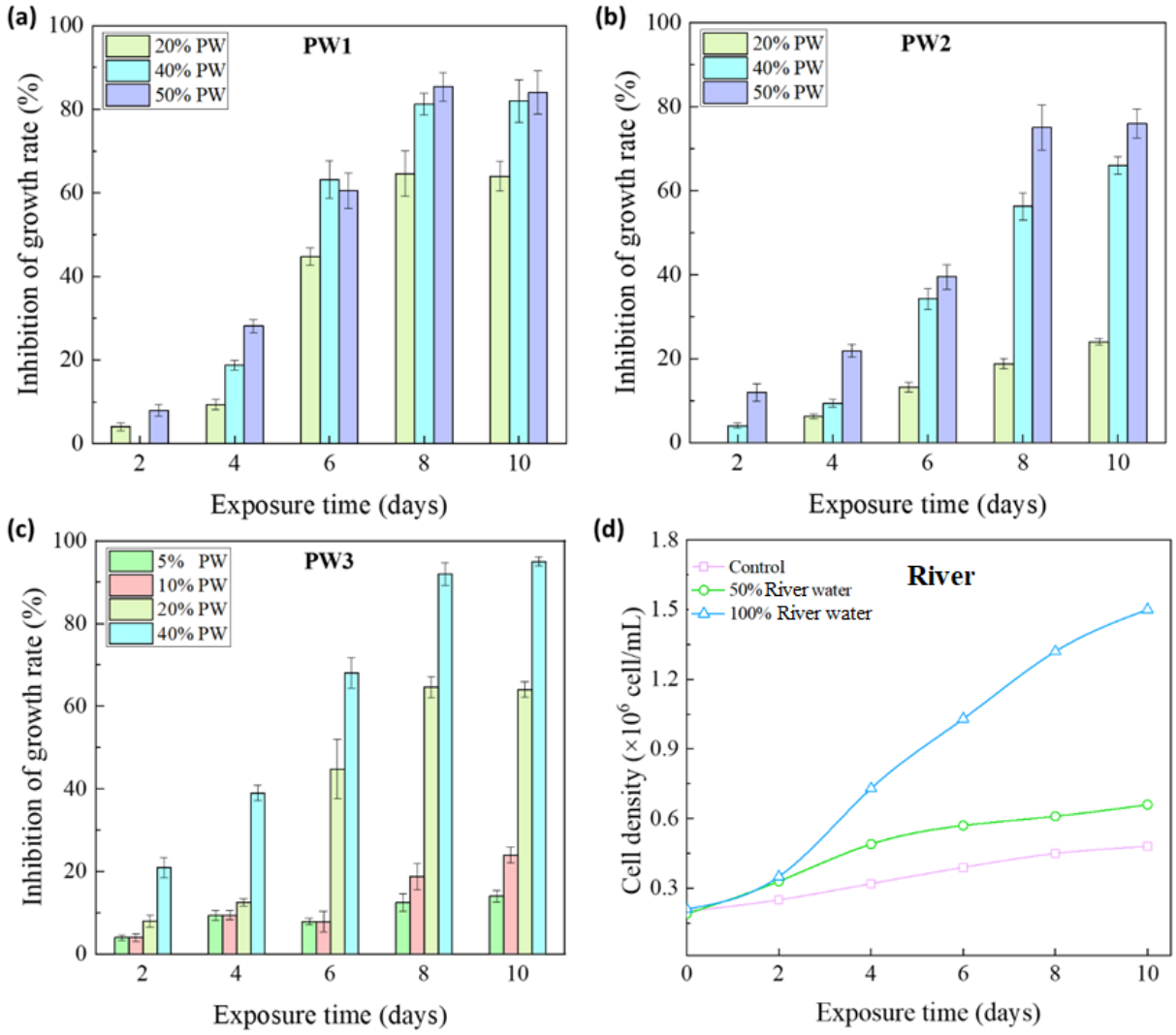

Fig. 9. Growth inhibition rate of *Selenastrum capricornutum* during 10-day exposure to different PW samples: (a) PW1, (b) PW2, (c) PW3; (d) growth curve of *Selenastrum capricornutum* during 10-day exposure to river water.

4. CONCLUSIONS

This study provided comprehensive analyses of PW samples from the Permian Basin, including over 300 targeted analytes and non-targeted analytes using FT ICR-MS. The microbial community structure of three PW samples was characterized by genomic DNA (gDNA) extraction and next generation sequencing. A suite of *in vitro* toxicity assays using various aquatic organisms (a marine luminescent bacterium *Vibrio fischeri* and freshwater microalgae *Scenedesmus obliquus* and *Selenastrum capricornutum*) were developed to investigate the toxicological characterizations of PW samples. Additional water samples were collected from the Pecos River, groundwater, and local drinking water sources in the Permian Basin for comparison.

The results show the PW samples from unconventional O&G operations in the Permian Basin have high concentrations of TDS, TOC, and ammonia, with mean values of 128,423 mg/L, 103.5 mg/L, and 432 mg/L, respectively. The PW quality is highly variable and TDS has a wide range of concentrations from 100,000 to 201,000 mg/L, and the concentration of Cl^- and Na^+ correspond to 62.1 % and 31.3% wt.% of the TDS. The total Ra (Ra-226 + Ra-228) has an average level of 195 pCi/L, which is much higher than the EPA regulatory limit of 5 pCi/L for drinking water. The targeted organic analysis detected 28 organic compounds (not including DRO, GRO, and MRO) in the PW samples. The detected VOCs include benzene, toluene, ethylbenzene, and xylene (BTEX), of which benzene, toluene, and xylene had the highest relative abundances. For the general SVOCs, phenol and pyridine had the highest relative abundance. There were 221 inorganic and organic constituents not detected in the PW samples. The high-resolution FT ICR-MS found that the Permian Basin PW samples have dominant organic compounds with DBE values from 3 to 7. A higher DBE value is indicative of greater aromaticity and less saturation.

The taxonomic compositions (phylum, class, order, family, and genus levels) showed the three PW samples had a similar bacterial community structure. At the phylum level, the most abundant phyla in PW samples were *Proteobacteria* (57.5%~67.2%) and *Firmicutes* (28.6%~37.1%). *Gammaproteobacteria* and *Clostridia* were the predominant classes in PW with relative abundances of 50.0%~59.3% and 23.6%~36.5%, respectively.

The *in vitro* toxicity study indicated the EC_{50} values of PW samples for *Vibrio fischeri* were in the range of 23%-30%. The chronic toxicity tests showed the EC_{50} values of PW samples were in the range of 8%-31% for *Scenedesmus obliquus*, and 15%-36% for *Selenastrum capricornutum*, and the toxicity varied for different PW samples.

The results generated from this study could enhance the understanding of the potential toxicological impacts of PW on aquatic ecosystems and the relationships between the chemical profiles and observed toxicity in PW. This study provides valuable data for understanding the environmental impacts of PW management, and to fill in the knowledge gap in PW characteristics for the potential beneficial use of PW as an alternative water source.

APPENDIX

Table A1. 221 organic and inorganic analytes not detected (ND) in the PW samples.

Analyte	Unit	Analyte	Unit
1,1,1-Trichloroethane	µg/L	Dieldrin	µg/L
1,1,2,2-Tetrachloroethane	µg/L	Diethyl phthalate	µg/L
1,1,2-Trichloroethane	µg/L	Dimethoate	µg/L
1,2,3-Trichlorobenzene	µg/L	Dimethyl phthalate	µg/L
1,2,4,5-Tetrachlorobenzene	µg/L	Di-n-butyl phthalate	µg/L
1,2,4-Trichlorobenzene	µg/L	Di-n-octyl phthalate	µg/L
1,2-Dichlorobenzene	µg/L	DONA (D-Glucosamine sulfate)	ng/L
1,2-Dichloropropane	µg/L	Endosulfan II	µg/L
1,2-Diphenylhydrazine (as Azobenzene)	µg/L	Endosulfan sulfate	µg/L
1,3,5-Trinitrobenzene	µg/L	Endrin aldehyde	µg/L
1,3-Dichlorobenzene	µg/L	Endrin ketone	µg/L
1,3-Dinitrobenzene	µg/L	Ethyl methanesulfonate	µg/L
1,4-Dichlorobenzene	µg/L	Europium	µg/L
1,4-Naphthoquinone	µg/L	F-53B Major	ng/L
10:2 FTS	ng/L	F-53B Minor	ng/L
1-Naphthylamine	µg/L	Famphur	µg/L
2,2'-oxybis[1-chloropropane]	µg/L	Fluoranthene	µg/L
2,3,4,6-Tetrachlorophenol	µg/L	Fluoride	mg/L
2,3,7,8-TCDD	pg/L	gamma-BHC (Lindane)	µg/L
2,4,5-Trichlorophenol	µg/L	Gold	µg/L
2,4,6-Trichlorophenol	µg/L	Heptachlor	µg/L
2,4-Dichlorophenol	µg/L	Heptachlor epoxide	µg/L
2,4-Dinitrophenol	µg/L	Hexachlorobenzene	µg/L
2,4-Dinitrotoluene	µg/L	Hexachlorobutadiene	µg/L
2,6-Dichlorophenol	µg/L	Hexachlorocyclopentadiene	µg/L
2,6-Dinitrotoluene	µg/L	Hexachloroethane	µg/L
2-Acetylaminofluorene	µg/L	Hexachloropropene	µg/L
2-Chloroethyl vinyl ether	µg/L	HFPO-DA (GenX)	ng/L
2-Chloronaphthalene	µg/L	Indeno[1,2,3-cd] pyrene	µg/L
2-Chlorophenol	µg/L	Isodrin	µg/L
2-Ethyl-1-Hexanol	µg/L	Isophorone	µg/L
2-Naphthylamine	µg/L	Isosafrole	µg/L
2-Nitroaniline	µg/L	Isovaleric acid	µg/L
2-Picoline	µg/L	Kepone	µg/L

3,3'-Dichlorobenzidine	µg/L	Lanthanum	µg/L
3-Methylcholanthrene	µg/L	Lead	µg/L
3-Nitroaniline	µg/L	Mercury	µg/L
4,4'-DDD	µg/L	Methapyrilene	µg/L
4,4'-DDE	µg/L	Methoxychlor	µg/L
4,4'-DDT	µg/L	Methyl methanesulfonate	µg/L
4,6-Dinitro-2-methylphenol	µg/L	Methyl parathion	µg/L
4:2 FTS	ng/L	Methylene Chloride	µg/L
4-Aminobiphenyl	µg/L	Molybdenum	µg/L
4-Bromophenyl phenyl ether	µg/L	Neodymium	µg/L
4-Chloro-3-methylphenol	µg/L	NEtFOSA	ng/L
4-Chloroaniline	µg/L	NEtFOSE	ng/L
4-Chlorophenyl phenyl ether	µg/L	N-ethylperfluorooctanesulfonamidoacetic acid (NEtFOSAA)	ng/L
4-Nitroaniline	µg/L	Nickel	µg/L
4-Nitroquinoline-1-oxide	µg/L	Nitrate as N	mg/L
4-tert-Octylphenol	ng/L	Nitrobenzene	µg/L
5-Nitro-o-toluidine	µg/L	NMeFOSA	ng/L
6:2 FTS	ng/L	NMeFOSE	ng/L
8:2 FTS	ng/L	N-methylperfluorooctanesulfonamidoacetic acid (NMeFOSAA)	ng/L
a,a-Dimethylphenethylamine	µg/L	N-Nitrosodiethylamine	µg/L
Acenaphthene	µg/L	N-Nitrosodimethylamine	µg/L
Acenaphthylene	µg/L	N-Nitrosodi-n-butylamine	µg/L
Acetophenone	µg/L	N-Nitrosodi-n-propylamine	µg/L
Acrolein	µg/L	N-Nitrosodiphenylamine	µg/L
Acrylamide	µg/L	N-Nitrosomethylethylamine	µg/L
Acrylonitrile	µg/L	N-Nitrosomorpholine	µg/L
Aldrin	µg/L	N-Nitrosopiperidine	µg/L
Aniline	µg/L	N-Nitrosopyrrolidine	µg/L
Antimony	µg/L	Nonylphenol	ng/L
Aramite	µg/L	Nonylphenol diethoxylate	ng/L
Aramite Peak 1	µg/L	Nonylphenol monoethoxylate	ng/L
Aramite Peak 2	µg/L	o-Toluidine	µg/L
Aramite, Total	µg/L	Parathion	µg/L
Aroclor-1016	µg/L	p-Dimethylamino azobenzene	µg/L
Aroclor-1221	µg/L	Pentachlorobenzene	µg/L
Aroclor-1232	µg/L	Pentachloroethane	µg/L
Aroclor-1242	µg/L	Pentachloronitrobenzene	µg/L
Aroclor-1248	µg/L	Pentachlorophenol	µg/L

Aroclor-1254	µg/L	Perfluorodecanesulfonic acid (PFDS)	ng/L
Aroclor-1260	µg/L	Perfluorodecanoic acid (PFDA)	ng/L
Arsenic	µg/L	Perfluorododecanesulfonic acid (PFDoS)	ng/L
Benzidine	µg/L	Perfluorododecanoic acid (PFDoA)	ng/L
Benzo[a]anthracene	µg/L	Perfluoroheptanesulfonic Acid (PFHpS)	ng/L
Benzo[a]pyrene	µg/L	Perfluoroheptanoic acid (PFHpA)	ng/L
Benzo[b]fluoranthene	µg/L	Perfluorohexanoic acid (PFHxA)	ng/L
Benzo[g,h,i]perylene	µg/L	Perfluorononanesulfonic acid (PFNS)	ng/L
Benzo[k]fluoranthene	µg/L	Perfluorononanoic acid (PFNA)	ng/L
Benzyl alcohol	µg/L	Perfluorooctanesulfonamide (FOSA)	ng/L
Beryllium	µg/L	Perfluorooctanesulfonic acid (PFOS)	ng/L
beta-BHC	µg/L	Perfluorooctanoic acid (PFOA)	ng/L
Bis(2-chloroethoxy)methane	µg/L	Perfluoropentanesulfonic acid (PFPeS)	ng/L
Bis(2-chloroethyl)ether	µg/L	Perfluoropentanoic acid (PFPeA)	ng/L
Bis(2-ethylhexyl) phthalate	µg/L	Perfluorotridecanoic acid (PFTriA)	ng/L
Bisphenol-A	ng/L	Perfluoroundecanoic acid (PFUnA)	ng/L
Bromoform	µg/L	Phenacetin	µg/L
Bromomethane	µg/L	Phorate	µg/L
Butyl benzyl phthalate	µg/L	p-Phenylene diamine	µg/L
Carbazole	µg/L	Pronamide	µg/L
Carbon tetrachloride	µg/L	Propylene glycol	mg/L
Chlordane (technical)	µg/L	Pyrene	µg/L
Chlorobenzene	µg/L	Safrole	µg/L
Chlorobenzilate	µg/L	Selenium	µg/L
Chlorodibromomethane	µg/L	Silver	µg/L
Chloroethane	µg/L	Sulfotepp	µg/L
Chloroform	µg/L	Tetrachloroethene	µg/L
Chloromethane	µg/L	Thallium	µg/L
Chromium	µg/L	Thionazin	µg/L
Chrysene	µg/L	Toxaphene	µg/L
cis-1,2-Dichloroethene	µg/L	trans-1,2-Dichloroethene	µg/L
cis-1,3-Dichloropropene	µg/L	trans-1,3-Dichloropropene	µg/L
Copper	µg/L	Trichloroethene	µg/L
Cr (VI)	mg/L	Trichlorofluoromethane	µg/L
delta-BHC	µg/L	Vinyl chloride	µg/L
Diallate	µg/L	Yttrium	µg/L
Dibenz(a,h)anthracene	µg/L	Zinc	µg/L
Dibenzofuran	µg/L	o,o',o"-Triethylphosphorothioate	µg/L
Dichlorobromomethane	µg/L		

REFERENCES

Burden, S., Fleming, M., Frithsen, J., Hills, L., Klewicki, K. and Knightes, C. 2016. Hydraulic fracturing for oil and gas: Impacts from the hydraulic fracturing water cycle on drinking water resources in the United States. Washington, DC: US EPA.

Carothers, W.W. and Kharaka, Y.K. 1978. Aliphatic acid anions in oil-field waters—implications for origin of natural gas. AAPG Bulletin 62(12), 2441-2453.

Centers for Disease Control and Prevention 2019. Polycyclic aromatic hydrocarbons (PAHs) factsheet.

Chaudhary, B.K., Sabie, R., Engle, M.A., Xu, P., Willman, S. and Carroll, K.C. 2019. Spatial variability of produced-water quality and alternative-source water analysis applied to the Permian Basin, USA. Hydrogeology Journal 27(8), 2889-2905.

Chen, L., Xu, P., Kota, K., Kuravi, S. and Wang, H. 2021. Solar distillation of highly saline produced water using low-cost and high-performance carbon black and airlaid paper-based evaporator (CAPER). Chemosphere 269, 129372.

Chen, L., Xu, P. and Wang, H. 2022. Photocatalytic membrane reactors for produced water treatment and reuse: Fundamentals, affecting factors, rational design, and evaluation metrics. Journal of Hazardous Materials 424, 127493.

Cho, Y., Jin, J.M., Witt, M., Birdwell, J.E., Na, J.-G., Roh, N.-S. and Kim, S. 2013. Comparing Laser Desorption Ionization and Atmospheric Pressure Photoionization Coupled to Fourier Transform Ion Cyclotron Resonance Mass Spectrometry to Characterize Shale Oils at the Molecular Level. Energy & Fuels 27(4), 1830-1837.

Dahm, K.G., Van Straaten, C.M., Munakata-Marr, J. and Drewes, Jr., E. 2013. Identifying well contamination through the use of 3-D fluorescence spectroscopy to classify coalbed methane produced water. Environmental science & technology 47(1), 649-656.

Danforth, C., Chiu, W.A., Rusyn, I., Schultz, K., Bolden, A., Kwiatkowski, C. and Craft, E. 2020. An integrative method for identification and prioritization of constituents of concern in produced water from onshore oil and gas extraction. Environment international 134, 105280.

Engle, M.A., Reyes, F.R., Varonka, M.S., Orem, W.H., Ma, L., Ianno, A.J., Schell, T.M., Xu, P. and Carroll, K.C. 2016. Geochemistry of formation waters from the Wolfcamp and "Cline" shales: Insights into brine origin, reservoir connectivity, and fluid flow in the Permian Basin, USA. Chemical Geology 425, 76-92.

Fisher, R.S. 1998. Geologic and geochemical controls on naturally occurring radioactive materials (NORM) in produced water from oil, gas, and geothermal operations. Environmental Geosciences 5(3), 139-150.

Folkerts, E.J., Blewett, T.A., He, Y. and Goss, G.G. 2017. Cardio-respirometry disruption in zebrafish (Danio rerio) embryos exposed to hydraulic fracturing flowback and produced water. Environ. Pollut. 231, 1477-1487.

FracFocus 2021. Chemical Names & CAS Registry Numbers.

Geza, M., Ma, G., Kim, H., Cath, T.Y. and Xu, P. 2018. iDST: An integrated decision support tool for treatment and beneficial use of non-traditional water supplies – Part I. Methodology. Journal of Water Process Engineering 25, 236-246.

GWPC 2019. Produced Water Report: Regulations, Current Practices, and Research Needs.

Hanor, J.S. 1994. Origin of saline fluids in sedimentary basins. Geological Society, London, Special Publications 78(1), 151-174.

He, Y., Flynn, S.L., Folkerts, E.J., Zhang, Y., Ruan, D., Alessi, D.S., Martin, J.W. and Goss, G.G. 2017. Chemical and toxicological characterizations of hydraulic fracturing flowback and produced water. Water Res. 114, 78-87.

Hickenbottom, K.L., Hancock, N.T., Hutchings, N.R., Appleton, E.W., Beaudry, E.G., Xu, P. and Cath, T.Y. 2013. Forward osmosis treatment of drilling mud and fracturing wastewater from oil and gas operations. Desalination 312(0), 60-66.

Hildenbrand, Z.L., Santos, I.C., Liden, T., Carlton Jr, D.D., Varona-Torres, E., Martin, M.S., Reyes, M.L., Mulla, S.R. and Schug, K.A. 2018. Characterizing variable biogeochemical changes during the treatment of produced oilfield waste. Science of the Total Environment 634, 1519-1529.
Hu, L., Wang, H., Xu, P. and Zhang, Y. 2021. Biomineralization of hypersaline produced water using microbially induced calcite precipitation. Water Research 190, 116753.
Hu, L., Yu, J., Luo, H., Wang, H., Xu, P. and Zhang, Y. 2020. Simultaneous recovery of ammonium, potassium and magnesium from produced water by struvite precipitation. Chemical Engineering Journal 382, 123001.
Huang, X., Zhou, H., Liang, Y., Li, Y., Xie, Q., Zhang, C. and You, S. 2020. Enhanced Bioremediation of Hydraulic Fracturing Flowback and Produced Water Using an Indigenous Biosurfactant-Producing Bacteria Acinetobacter sp. Y2. Chem. Eng. J., 125348.
IHS Markit 2020. Produced Water from Onshore US Oil and Gas Activities to Decline to Nearly 20 Billion Barrels Annually; Reach $28 Billion in Value by 2022, IHS Markit Says IHS Markit.
Jackson, E.C. 2014. Hydraulic fracturing: a look at efficiency in the Haynesville Shale and the environmental effects of fracking, Louisiana State University.
Jiang, W., Lin, L., Gedara, S.H., Schaub, T.M., Jarvis, J.M., Wang, X., Xu, X., Nirmalakhandan, N. and Xu, P. 2020. Potable-quality water recovery from primary effluent through a coupled algal-osmosis membrane system. Chemosphere 240, 124883.
Jiang, W., Lin, L., Xu, X., Cheng, X., Zhang, Y., Hall, R. and Xu, P. 2021a. A Critical Review of Analytical Methods for Comprehensive Characterization of Produced Water. Water 13(2), 183.
Jiang, W., Pokharel, B., Lin, L., Cao, H., Carroll, K.C., Zhang, Y., Galdeano, C., Musale, D.A., Ghurye, G.L. and Xu, P. 2021b. Analysis and prediction of produced water quantity and quality in the Permian Basin using machine learning techniques. Science of The Total Environment, 149693.
Jin, J.M., Kim, S. and Birdwell, J.E. 2012. Molecular Characterization and Comparison of Shale Oils Generated by Different Pyrolysis Methods. Energy & Fuels 26(2), 1054-1062.
Kahrilas, G.A., Blotevogel, J., Corrin, E.R. and Borch, T. 2016. Downhole transformation of the hydraulic fracturing fluid biocide glutaraldehyde: implications for flowback and produced water quality. Environmental science & technology 50(20), 11414-11423.
Lester, Y., Ferrer, I., Thurman, E.M., Sitterley, K.A., Korak, J.A., Aiken, G. and Linden, K.G. 2015. Characterization of hydraulic fracturing flowback water in Colorado: implications for water treatment. Science of the total environment 512, 637-644.
Liang, R., Davidova, I.A., Marks, C.R., Stamps, B.W., Harriman, B.H., Stevenson, B.S., Duncan, K.E. and Suflita, J.M. 2016. Metabolic capability of a predominant Halanaerobium sp. in hydraulically fractured gas wells and its implication in pipeline corrosion. Frontiers in microbiology 7, 988.
Liden, T., Carlton Jr., D.D., Miyazaki, S., Otoyo, T. and Schug, K.A. 2019. Forward osmosis remediation of high salinity Permian Basin produced water from unconventional oil and gas development. Science of The Total Environment 653, 82-90.
Liden, T., Santos, I.C., Hildenbrand, Z.L. and Schug, K.A. 2018. Treatment modalities for the reuse of produced waste from oil and gas development. Science of the Total Environment 643, 107-118.
Lin, L., Jiang, W., Chen, L., Xu, P. and Wang, H. 2020. Treatment of produced water with photocatalysis: recent advances, affecting factors and future research prospects. Catalysts 10(8), 924.
Lipus, D., Vikram, A., Ross, D., Bain, D., Gulliver, D., Hammack, R. and Bibby, K. 2017. Predominance and metabolic potential of Halanaerobium spp. in produced water from hydraulically fractured Marcellus shale wells. Applied and environmental microbiology 83(8).
Luek, J.L. and Gonsior, M. 2017. Organic compounds in hydraulic fracturing fluids and wastewaters: a review. Water research 123, 536-548.
Ma, G., Geza, M., Cath, T.Y., Drewes, J.E. and Xu, P. 2018. iDST: An integrated decision support tool for treatment and beneficial use of non-traditional water supplies – Part II. Marcellus and Barnett Shale case studies. Journal of Water Process Engineering 25, 258-268.
Mazerov, K. 2013. Environmentally friendly proppant technology to improve hydraulic fracturing efficiency.

Navarro, L., Jones, M. and NMulhearn, S. 2016. Development of Risk-Based Comparison Levels for Chemicals in Agricultural Irrigation Water. Sponnsored by California Resources Corporation. .
Oecd, O. 1981. Guidelines for the Testing of Chemicals. Test Guideline 201.
Oetjen, K., Chan, K.E., Gulmark, K., Christensen, J.H., Blotevogel, J., Borch, T., Spear, J.R., Cath, T.Y. and Higgins, C.P. 2018. Temporal characterization and statistical analysis of flowback and produced waters and their potential for reuse. Science of the Total Environment 619, 654-664.
Olsson, O., Weichgrebe, D. and Rosenwinkel, K.-H. 2013. Hydraulic fracturing wastewater in Germany: composition, treatment, concerns. Environmental earth sciences 70(8), 3895-3906.
Rodriguez, A.Z., Wang, H., Hu, L., Zhang, Y. and Xu, P. 2020. Treatment of produced water in the permian basin for hydraulic fracturing: Comparison of different coagulation processes and innovative filter media. Water 12(3), 770.
Roper, W. 1992. Toxicological profile for pyridine. Agency for Toxic Substances and Disease Registry, US Public Health Service.
Scanlon, B.R., Ikonnikova, S., Yang, Q. and Reedy, R.C. 2020a. Will Water Issues Constrain Oil and Gas Production in the United States? Environmental science & technology 54(6), 3510-3519.
Scanlon, B.R., Reedy, R.C., Male, F. and Walsh, M. 2017. Water issues related to transitioning from conventional to unconventional oil production in the Permian Basin. Environmental science & technology 51(18), 10903-10912.
Scanlon, B.R., Reedy, R.C., Xu, P., Engle, M., Nicot, J., Yoxtheimer, D., Yang, Q. and Ikonnikova, S. 2020b. Can we beneficially reuse produced water from oil and gas extraction in the US? Science of The Total Environment 717, 137085.
Schenk, J., Carlton, D.D., Smuts, J., Cochran, J., Shear, L., Hanna, T., Durham, D., Cooper, C. and Schug, K.A. 2019. Lab-simulated downhole leaching of formaldehyde from proppants by high performance liquid chromatography (HPLC), headspace gas chromatography-vacuum ultraviolet (HS-GC-VUV) spectroscopy, and headspace gas chromatography-mass spectrometry (HS-GC-MS). Environmental Science: Processes & Impacts 21(2), 214-223.
Shaleexperts Permian Basin Geologic Breakdown.
Shrestha, N., Chilkoor, G., Wilder, J., Ren, Z.J. and Gadhamshetty, V. 2018. Comparative performances of microbial capacitive deionization cell and microbial fuel cell fed with produced water from the Bakken shale. Bioelectrochemistry 121, 56-64.
Thacker, J.B., Carlton, D.D., Hildenbrand, Z.L., Kadjo, A.F. and Schug, K.A. 2015. Chemical analysis of wastewater from unconventional drilling operations. Water 7(4), 1568-1579.
U.S.EIA 2021. Drilling Productivity Report.
U.S.EPA 2011. Proceedings of the Technical Workshops for the Hydraulic Fracturing Study: Chemical and Analytical Methods.
U.S.EPA 2020. Summary of Input on Oil and Gas Extraction Wastewater Management Practices Under the Clean Water Act Final Report.
USGS 2021. U.S. Geological Survey National Produced Waters Geochemical Database v2.3.
Veil, J. 2020. U.S. Produced Water Volumes and Management Practices in 2017.
Wang, C., Huang, Y., Zhang, Z., Hao, H. and Wang, H. 2020. Absence of the nahG-like gene caused the syntrophic interaction between Marinobacter and other microbes in PAH-degrading process. J. Hazard. Mater. 384, 121387.
Wang, H., Lu, L., Chen, X., Bian, Y. and Ren, Z.J. 2019. Geochemical and microbial characterizations of flowback and produced water in three shale oil and gas plays in the central and western United States. Water research 164, 114942.
Wang, X., Goual, L. and Colberg, P.J.S. 2012. Characterization and treatment of dissolved organic matter from oilfield produced waters. Journal of Hazardous Materials 217-218, 164-170.
Xu, P. and Drewes, J.E. 2006. Viability of nanofiltration and ultra-low pressure reverse osmosis membranes for multi-beneficial use of methane produced water. Separation and Purification Technology 52, 67-76.

Xu, P., Drewes, J.E. and Heil, D. 2008a. Beneficial use of co-produced water through membrane treatment: technical-economic assessment. Desalination 225(1-3), 139-155.
Xu, P., Drewes, J.E., Heil, D. and Wang, G. 2008b. Treatment of brackish produced water using carbon aerogel-based capacitive deionization technology. Water Research 40(10-11), 2605-2617.